

Molecular Microscopy: Fundamental Limitations

Abstract. On the basis of estimates of molecular damage caused by the observation process, it is concluded that molecular microscopy of biological molecules in which the individual atoms are resolved is impossible with an electron or x-ray microscope. Microscopes that use low-energy helium atoms or neutrons as illuminants may be capable of serving as ultimate biomolecular microscopes.

inal adenine (20). Although this does not prevent electron molecular microscopy if the observations are made sufficiently rapidly, considering the high state of ionization implied by "instantaneous" observation, the measurements would have to be made within a molecular vibration time of $\approx 10^{-18}$ second, which is far beyond present capabilities. The large values of R obviously preclude x-ray molecular microscopy.

Breedlove Jr, J. R., and G. T. Trammel. "Molecular microscopy: fundamental limitations." Science 170.3964 (1970): 1310-1313.

Nobel Symposium 158

Free Electron Laser Research

Inelastic scattering as a probe of elementary excitations in matter

Jerome Hastings

S. Glenzer Group

G. Monaco

G. Gregori

L. Fletcher

D. Reis group

M. Trigo

Crystal Dynamics and Inelastic Scattering of Neutrons

G. PLACZEK AND L. VAN HOVE

Institute for Advanced Study, Princeton, New Jersey

(Received December 10, 1953)

A general discussion is given for the angular and energy distribution of neutrons inelastically scattered by a crystal, with special emphasis on those features of the distribution in which the dynamical properties of the crystal manifest themselves most immediately. The direct relationship between the energy changes in scattering and the dispersion law of the crystal vibrations is analyzed. While for x-rays, due to the extremely small relative size of these energy changes, the dispersion law has to be inferred indirectly from intensity measurements, it is shown that the very much larger relative magnitude of energy transfers in the case of slow neutrons opens the possibility of direct determination of the frequency-wave vector relationship and the frequency-distribution function of the crystal vibrations by energy measurements on scattered neutrons. The general properties of the outgoing neutron distribution in momentum space which are relevant for this purpose are derived by first considering the particularly instructive limiting case of neutrons initially at rest and subsequently generalizing the results to incident neutrons of arbitrary energy.

Correlations in Space and Time and Born Approximation Scattering in Systems of Interacting Particles

LÉON VAN HOVE

Institute for Advanced Study, Princeton, New Jersey

(Received March 16, 1954)

A natural time-dependent generalization is given for the well-known pair distribution function $g(\mathbf{r})$ of systems of interacting particles. The pair distribution in space and time thus defined, denoted by $G(\mathbf{r},t)$, gives rise to a very simple and entirely general expression for the angular and energy distribution of Born approximation scattering by the system. This expression is the natural extension of the familiar Zernike-Prins formula to scattering in which the energy transfers are not negligible compared to the energy of the scattered particle. It is therefore of particular interest for scattering of slow neutrons by general systems of interacting particles: G is then the proper function in terms of which to analyze the scattering data.

After defining the G function and expressing the Born approximation scattering formula in terms of it, the paper studies its general properties and indicates its role for neutron scattering. The qualitative behavior of G for liquids and dense gases is then described and the long-range part exhibited by the function near the critical point is calculated. The explicit expression of G for crystals and for ideal quantum gases is briefly derived and discussed.

general expression for scattering cross section

$$\frac{d\sigma}{ds} = \frac{1}{\phi} \frac{1}{ds} \sum_{k'} W_{k\lambda - k'\lambda'}$$

where ϕ = flux of incident particles

$W_{k\lambda - k'\lambda'}$: number of transitions per second

from $k\lambda \rightarrow k'\lambda'$: $\lambda \rightarrow \lambda'$ transition
 $k \rightarrow k'$ of system
wave vector

$$\left(\frac{d^2\sigma}{d\Omega dE} \right) = \frac{\sigma_{coh}}{4\pi} \frac{k'}{k} \frac{1}{2\pi\hbar} \sum_{jj'} \langle \exp\{-ik \cdot R_{j'}(0)\} \rangle$$

$$\exp\{ik \cdot R_j(t)\} = \exp(-i\omega t) dt$$

define $I(k, t) = \frac{1}{N} \sum_{jj'} \langle \exp\{-ik \cdot R_{j'}(0)\} \rangle$

$$\exp\{ik \cdot R_j(t)\}$$

$$S(k, \omega) = \frac{1}{2\pi\hbar} \int I(k, t) \exp(-i\omega t) dt$$

NOW

$$\frac{d\sigma}{d\Omega dE} = \frac{\sigma_{coh}}{4\pi} \frac{k'}{k} N \cdot S(k, \omega)$$

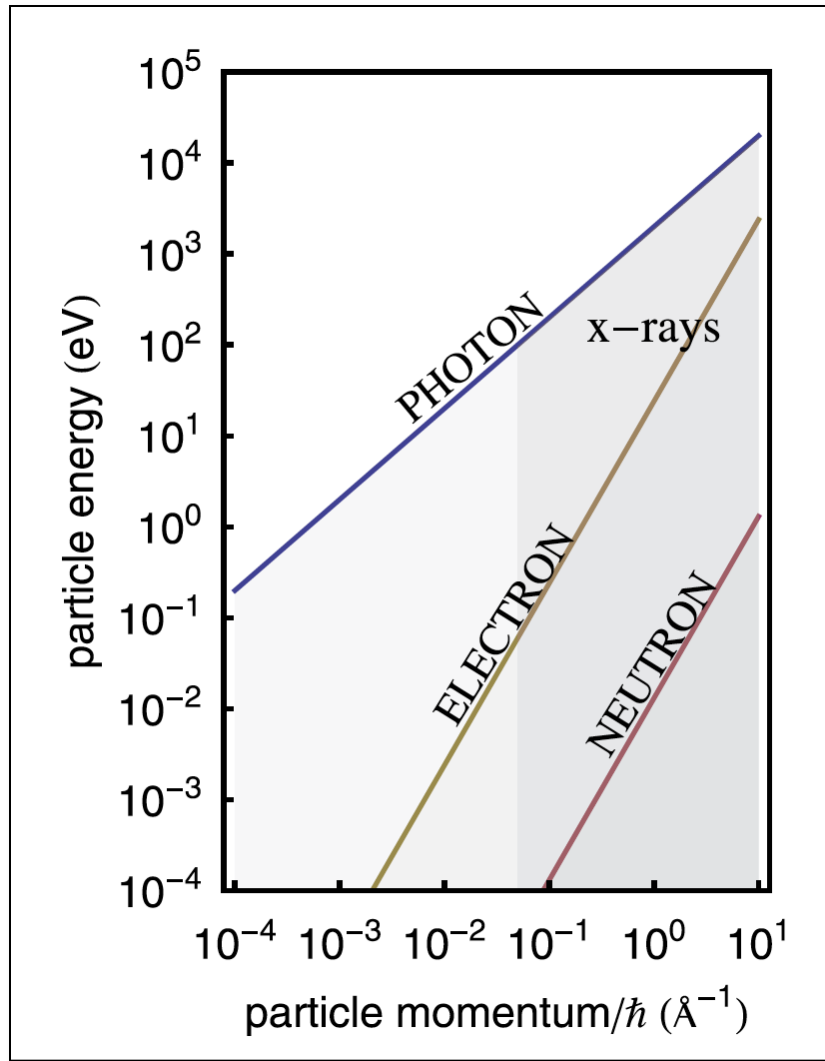
for x-rays $\Delta E \gg E_\gamma - E_X$, so

$$\frac{d\sigma}{d\Omega} = \frac{\sigma_{coh}}{4\pi} N \left\{ 1 + \int g(r) \exp[i k_\gamma r] dr \right\}$$

pair correlation func.

Energy – Momentum Relationship

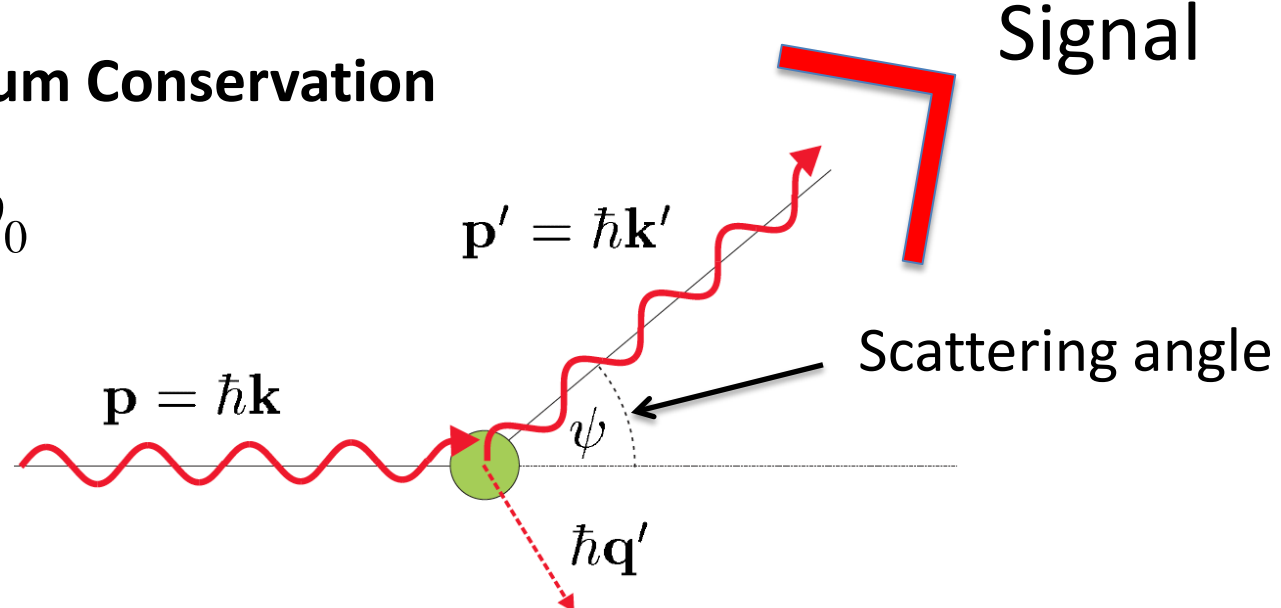
Photons, Electrons, Neutrons



Energy/Momentum Conservation

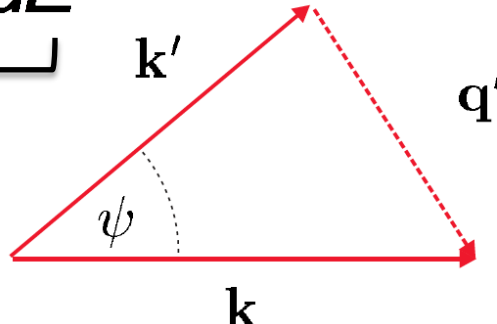
$$\Delta E = \hbar\omega - \hbar\omega_0$$

$$\vec{q}' = \vec{k} - \vec{k}'$$

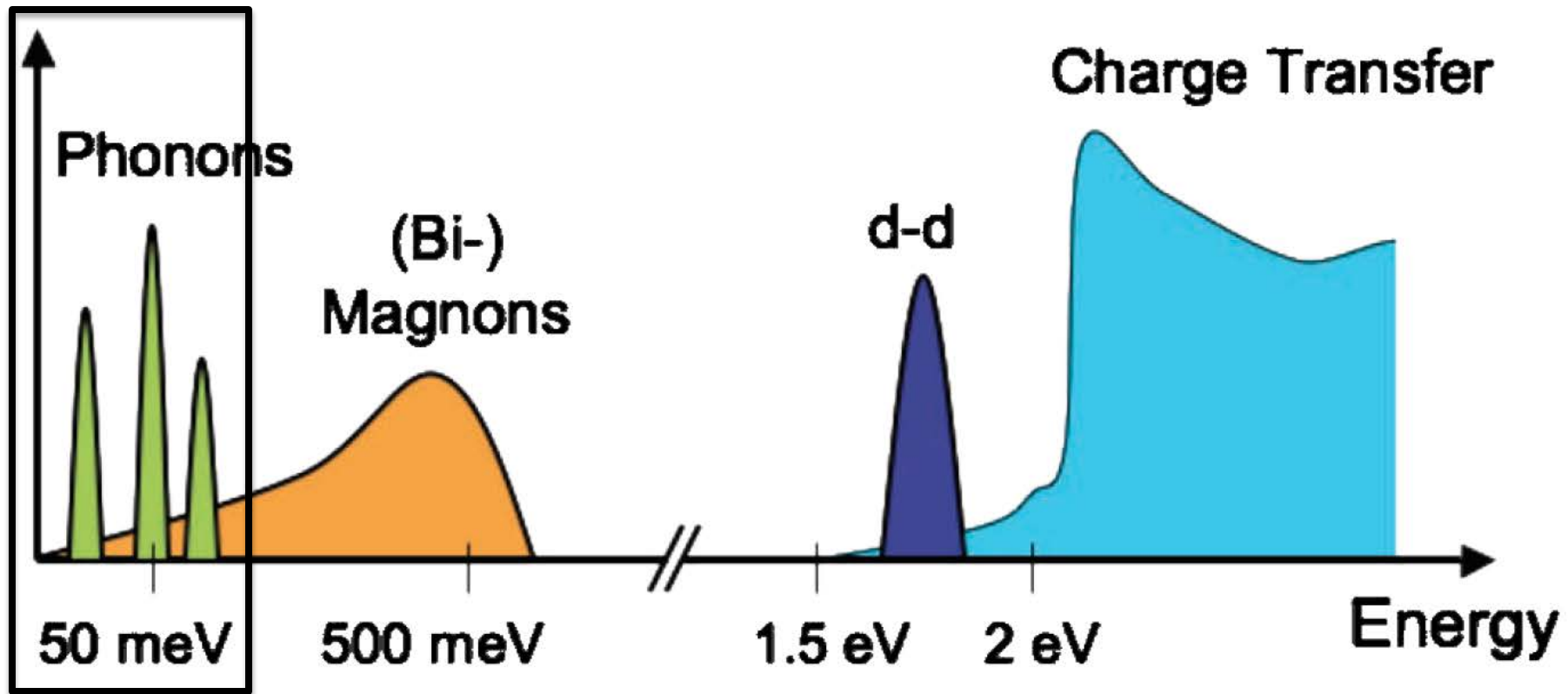


$$\text{Signal} = \frac{d^2\sigma}{d\Omega dE} \cdot N d\Omega dE$$

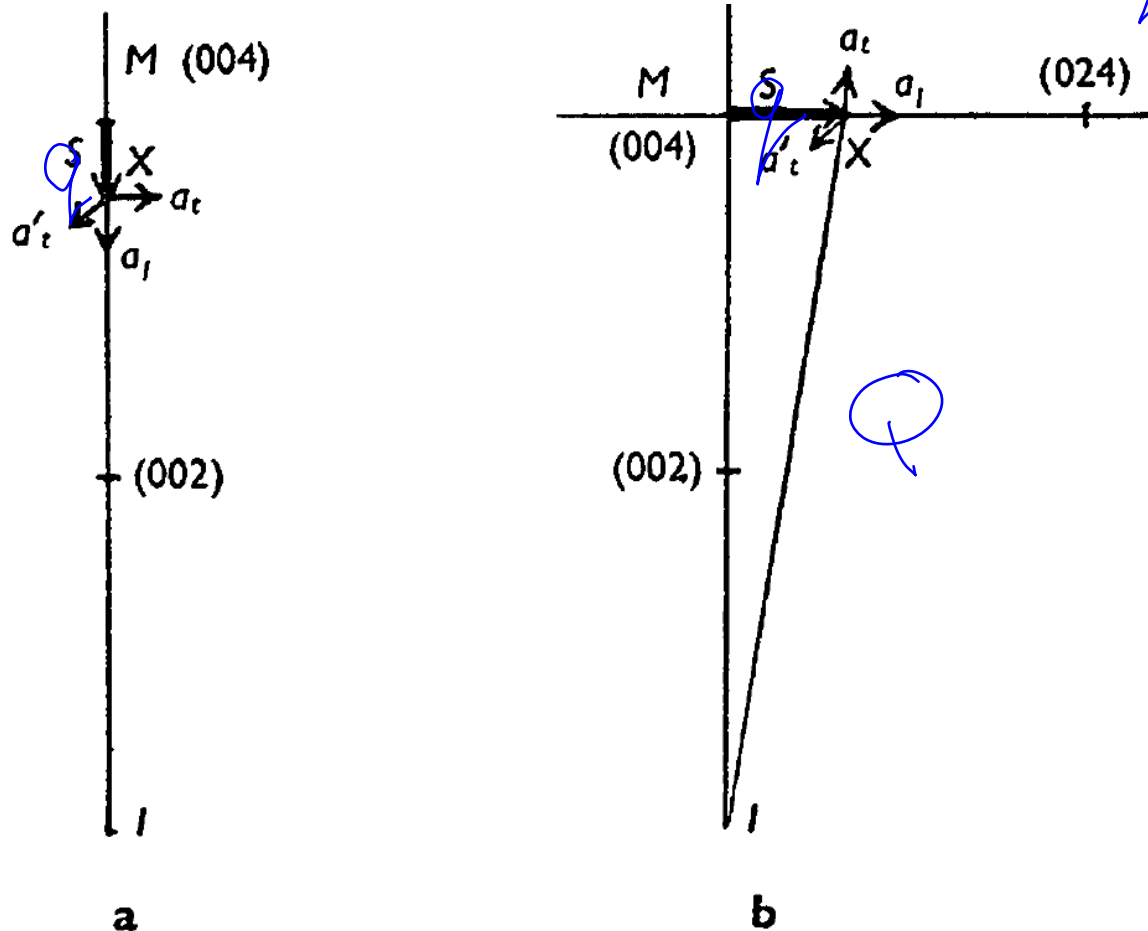
Instrument function



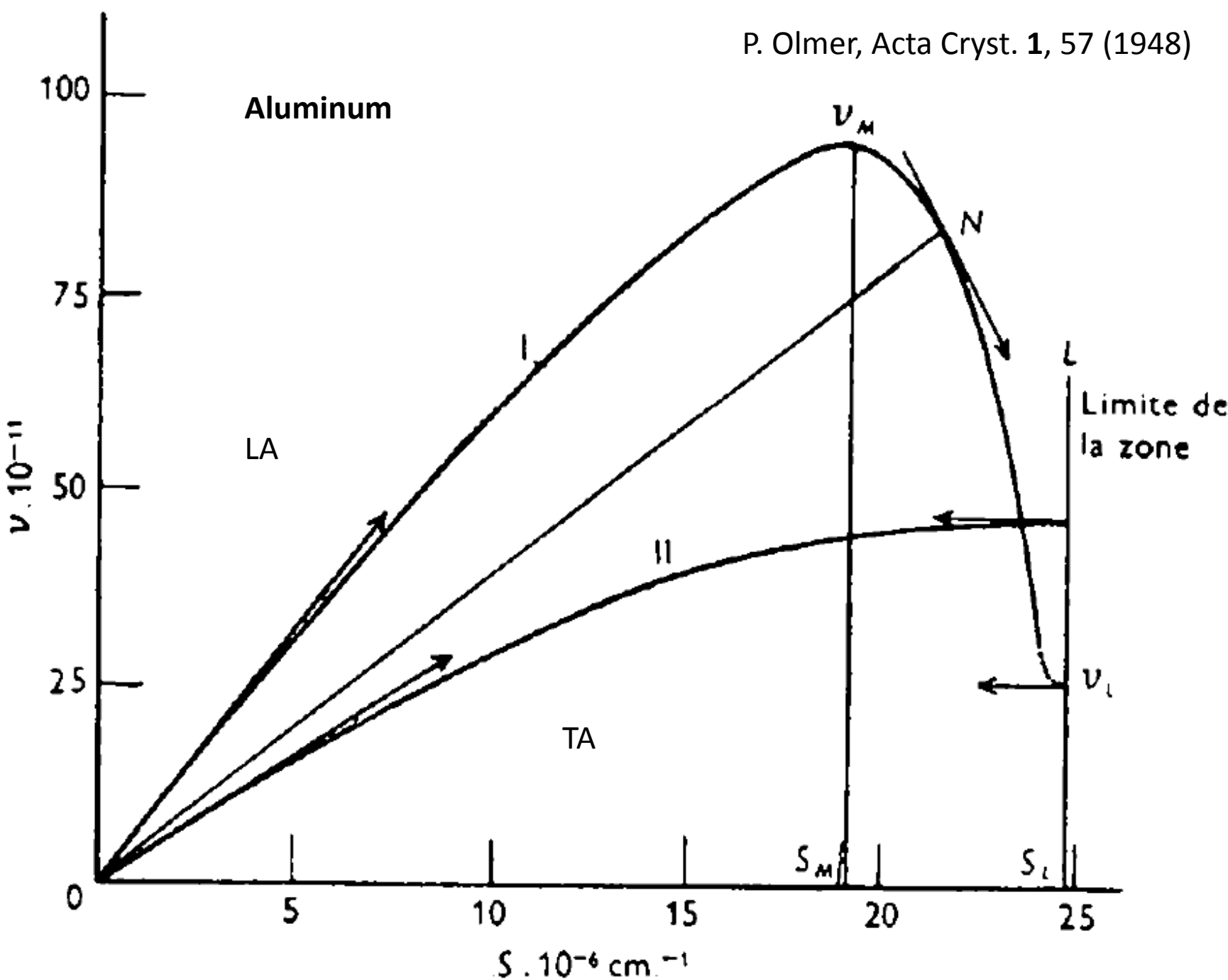
Elementary excitations in solids



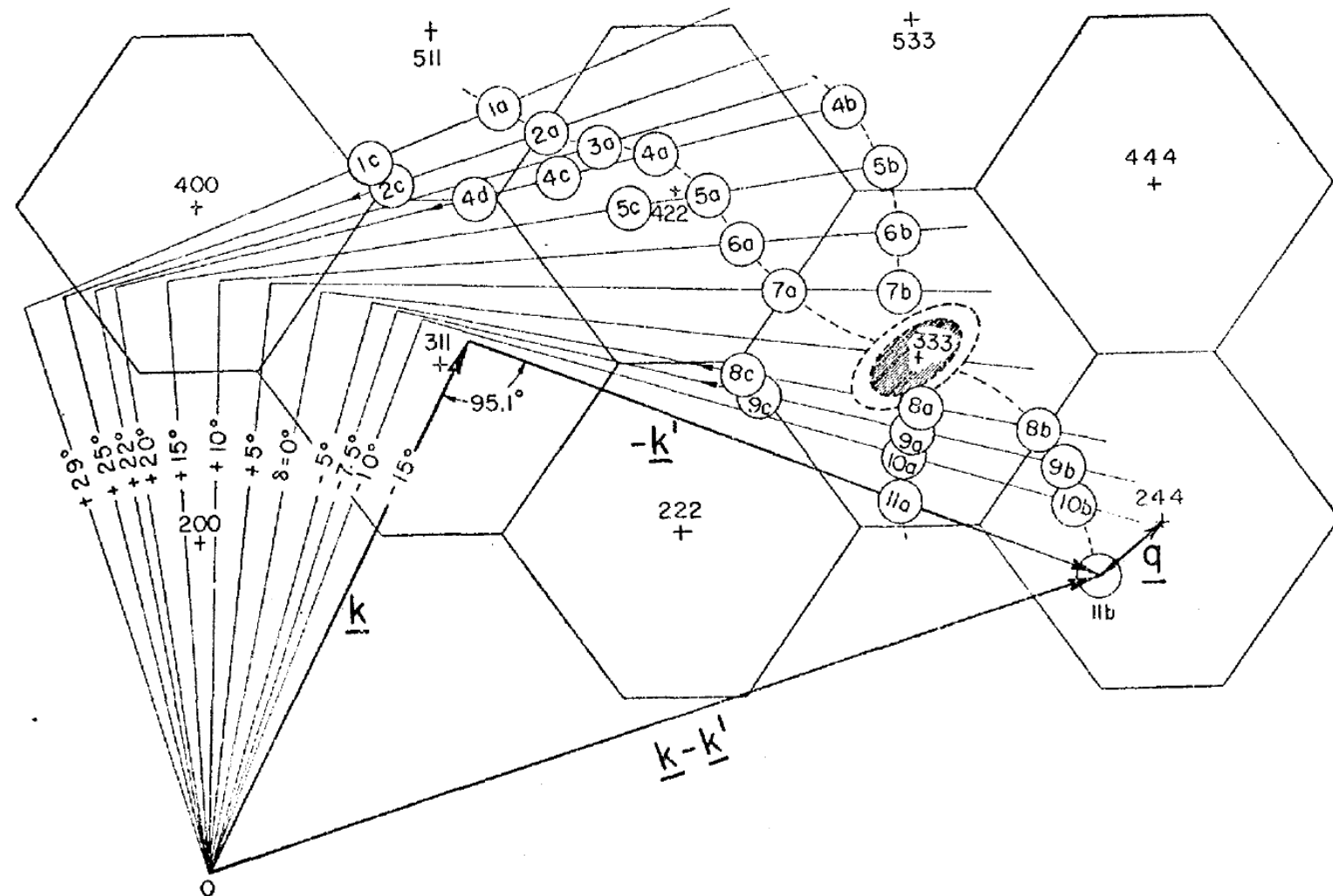
$$I(q) = f^2 \frac{e^{-2M}}{m} |Q^2| \sum_{j=1}^3 \frac{Eq_j^*(Q \cdot E)^2}{\lambda^2 q_j}$$



P. Olmer, Acta Cryst. 1, 57 (1948)

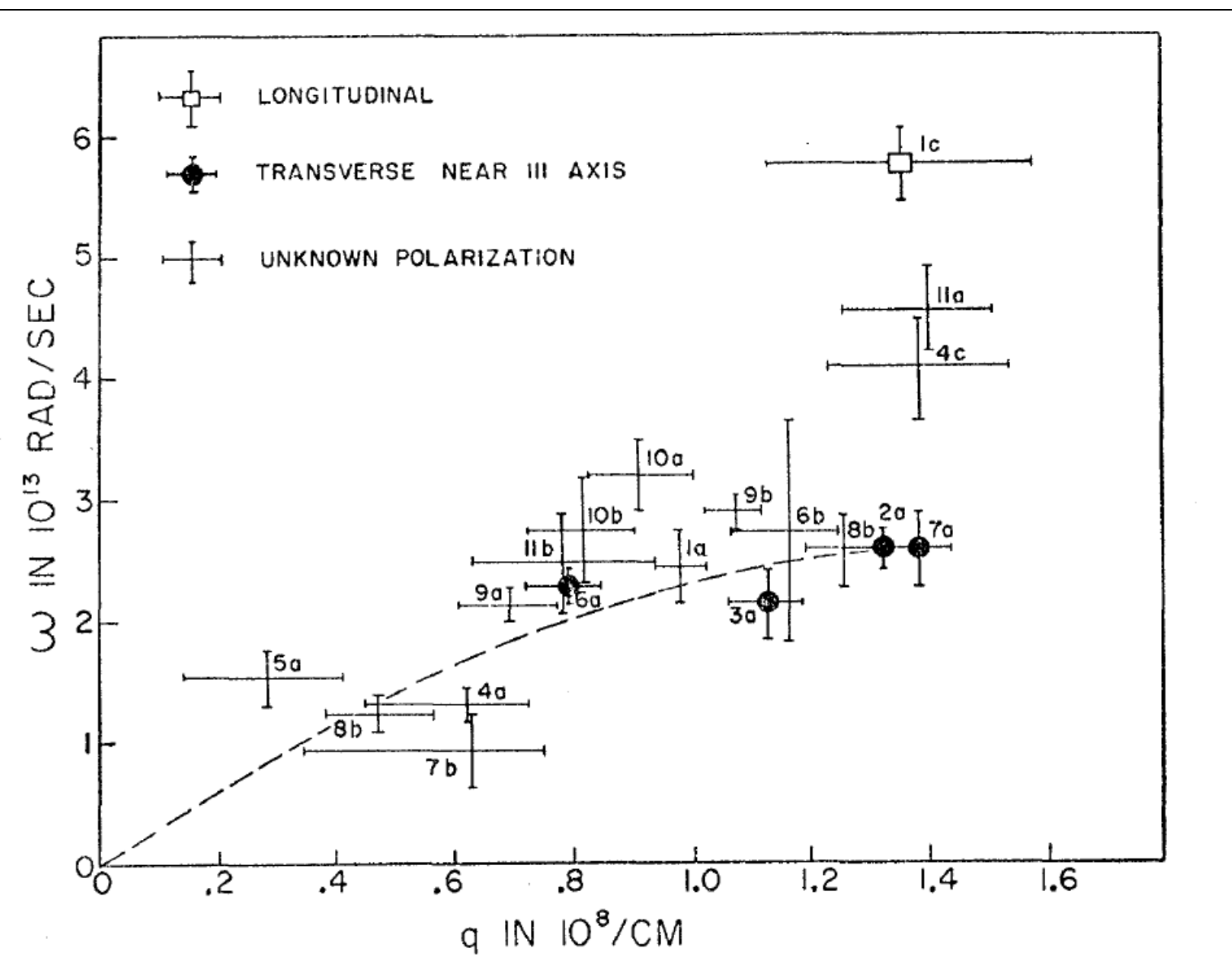


Neutron scattering geometry

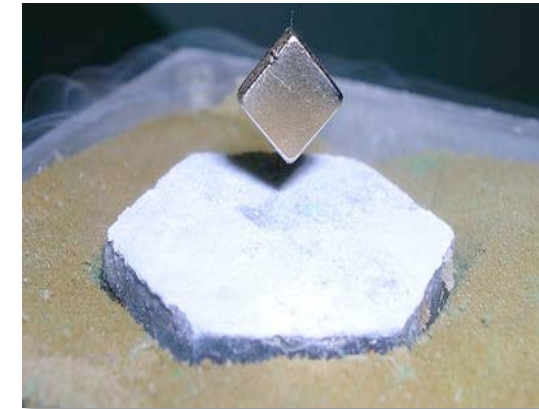


B. N. Brockhouse and A. T. Stewart, Phys. Rev. **100**, 756 (1955)

Dispersion in Aluminum



B. N. Brockhouse and A. T. Stewart, Phys. Rev. **100**, 756 (1955)



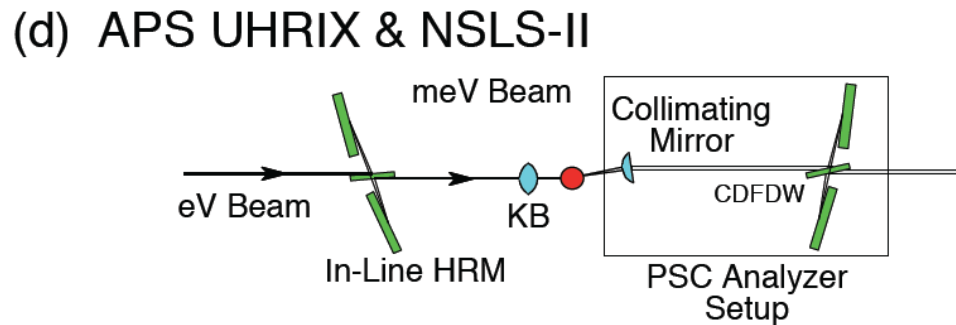
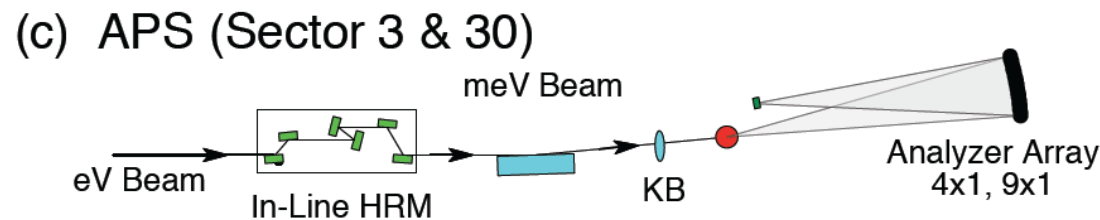
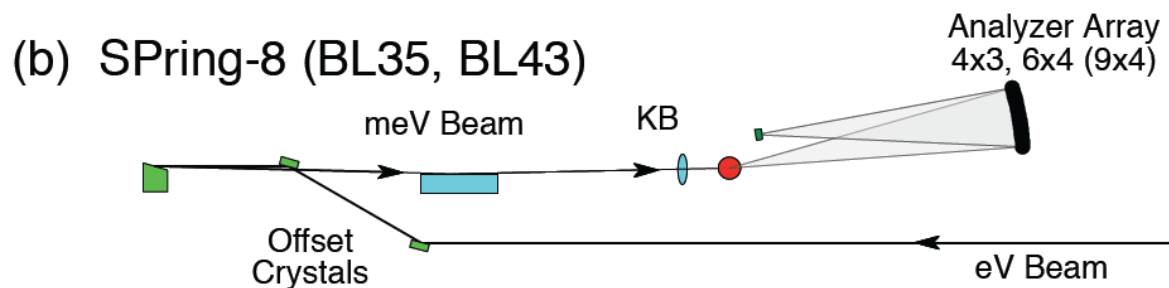
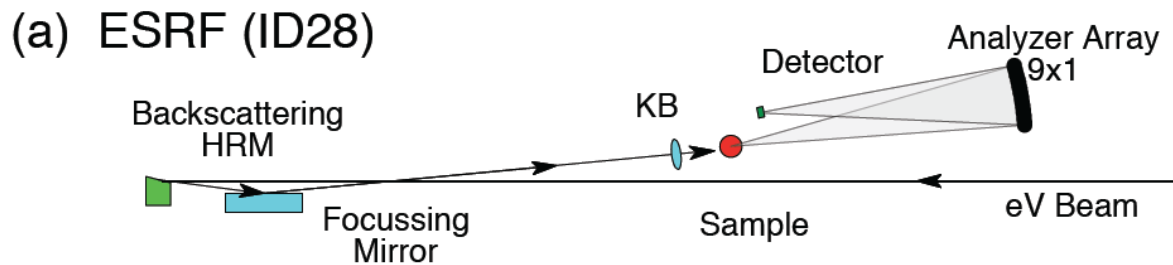
Time-domain Inelastic X-ray Scattering from Phonons

David A. Reis

Stanford PULSE Institute,

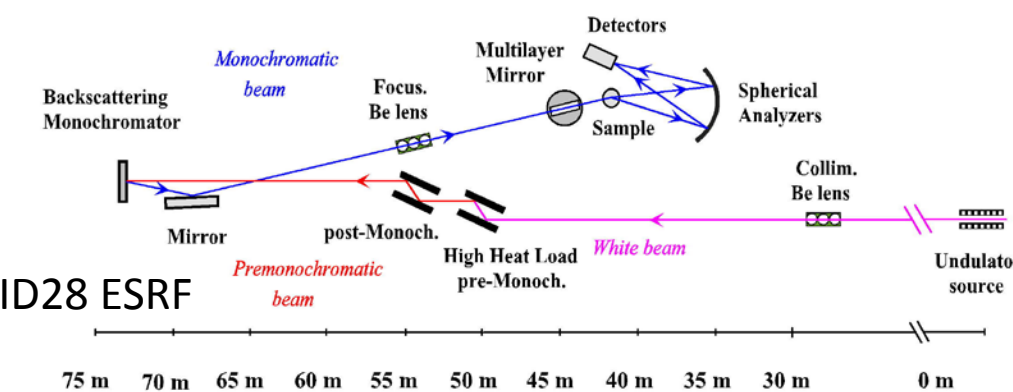
Applied Physics and Photon Science

Stanford University and SLAC National Accelerator Laboratory

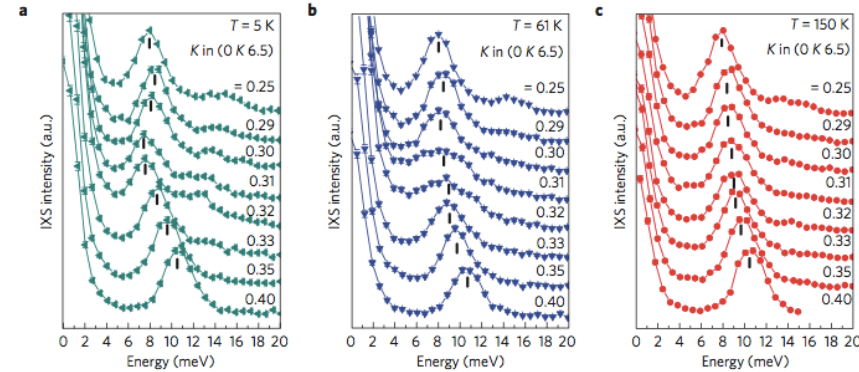


Inelastic X-ray Scattering:

$$S(\vec{Q}, \omega) \propto \sum_j \int dt e^{i\omega t} \langle u_{j,\vec{Q}}(0) u_{j,-\vec{Q}}(t) \rangle$$



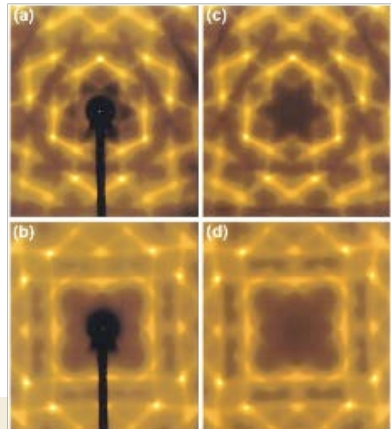
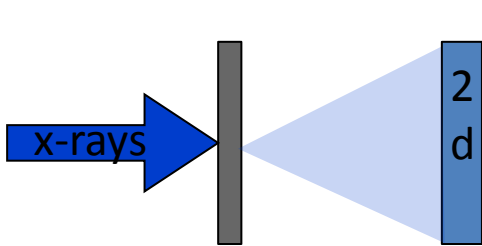
Underdoped YBCO



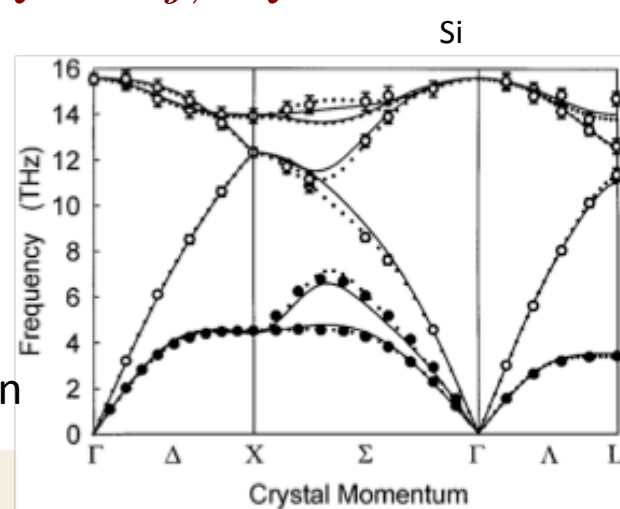
M. Le Tacon et. al, Nat. Phys. 10, 52 (2014)

X-ray Diffuse Scattering:

$$S(\vec{Q}) \propto \sum_j \langle u_{j,\vec{Q}}(0) u_{j,-\vec{Q}}(0) \rangle$$

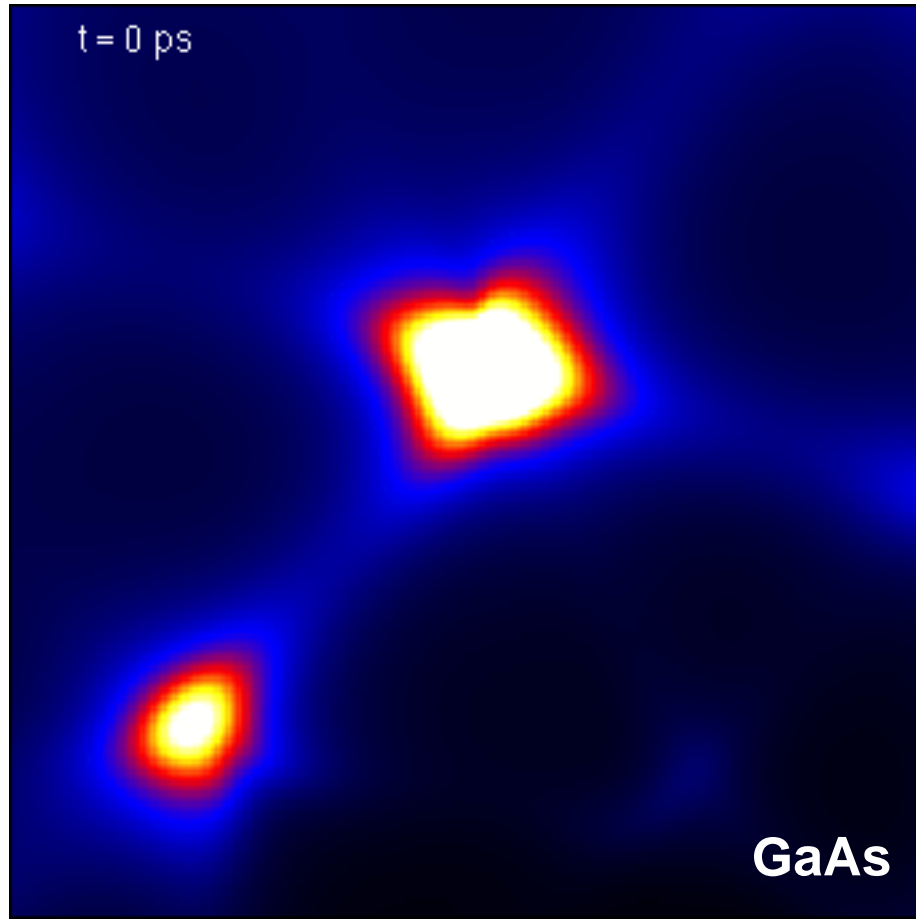


fit to Bose-Einstein distribution.

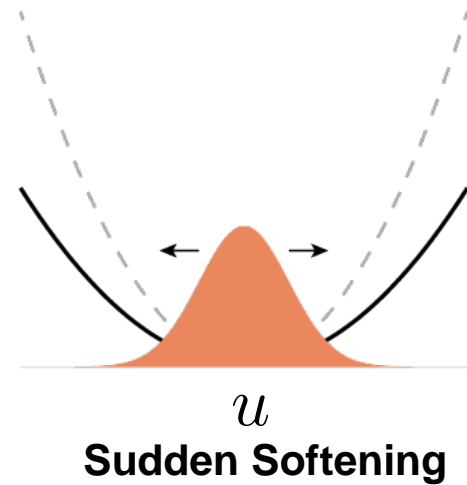


M. Holt et al., PRL 83 (1999).

Inducing temporal coherences on the noise



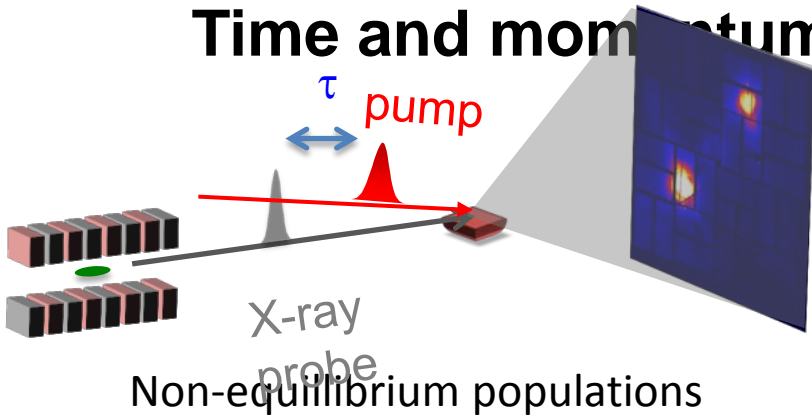
$$\left\langle (\vec{Q} \cdot u_{-\vec{q}}(t))(\vec{Q} \cdot u_{\vec{q}}(t)) \right\rangle$$



independent modes (oscillation at twice frequency):

$$\langle u_q u_{-q} \rangle = \frac{1}{4m\omega_q} \left(\left(1 + \frac{\omega_q^2}{\omega_q^{2\prime}} \right) + \left(1 - \frac{\omega_q^{2\prime}}{\omega_q^2} \right) \cos(2\omega'\tau) \right)$$

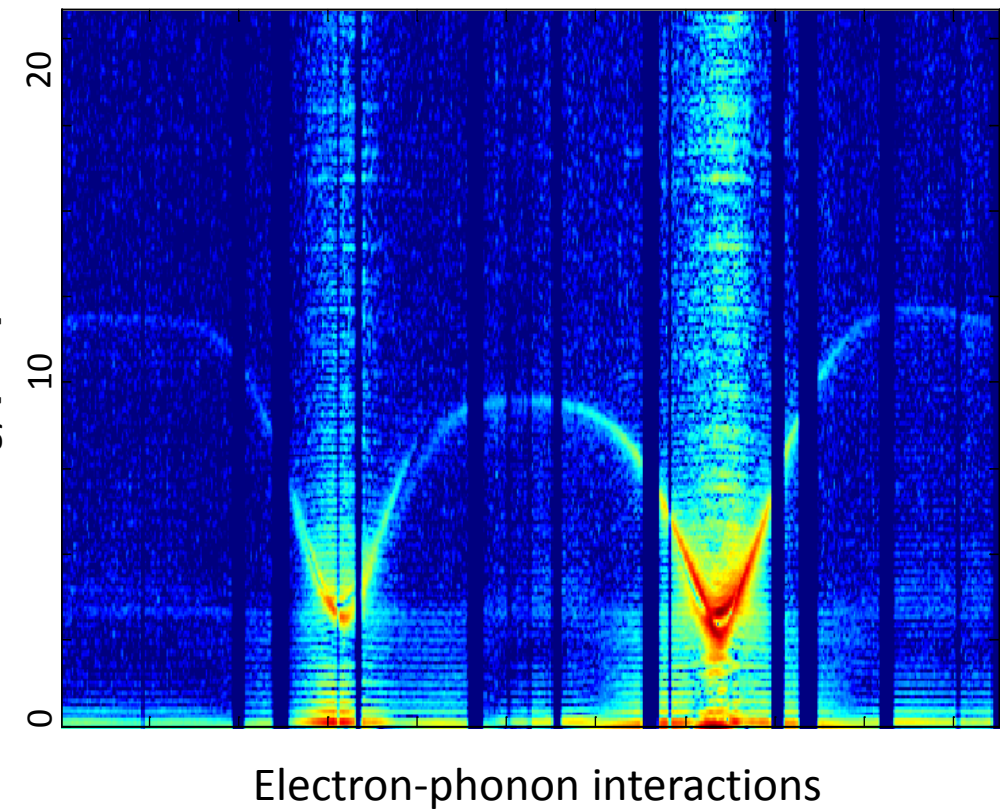
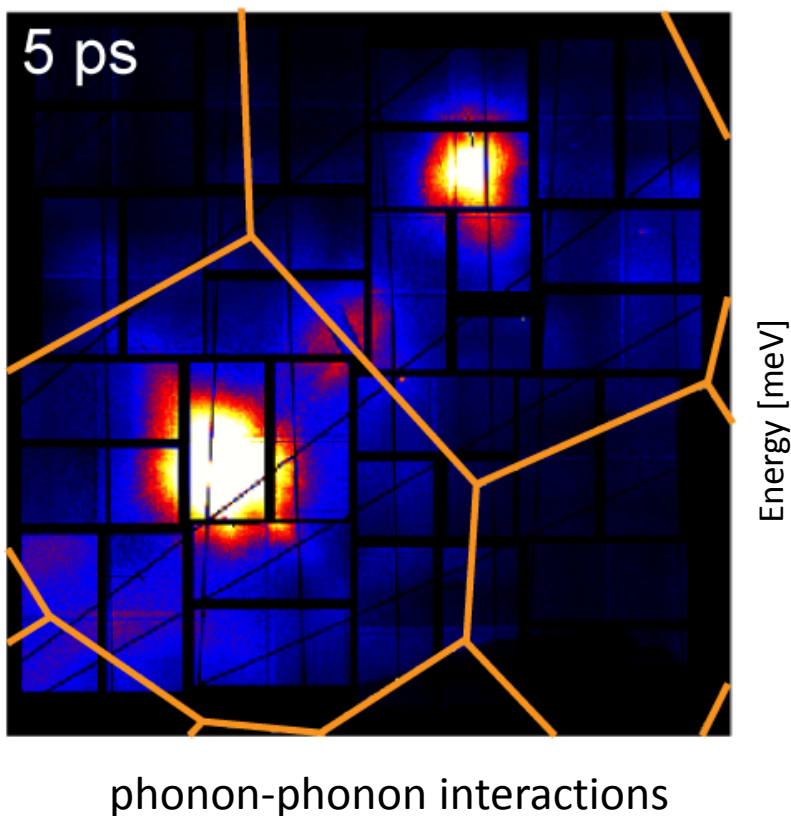
Time and momentum-domain x-ray scattering:



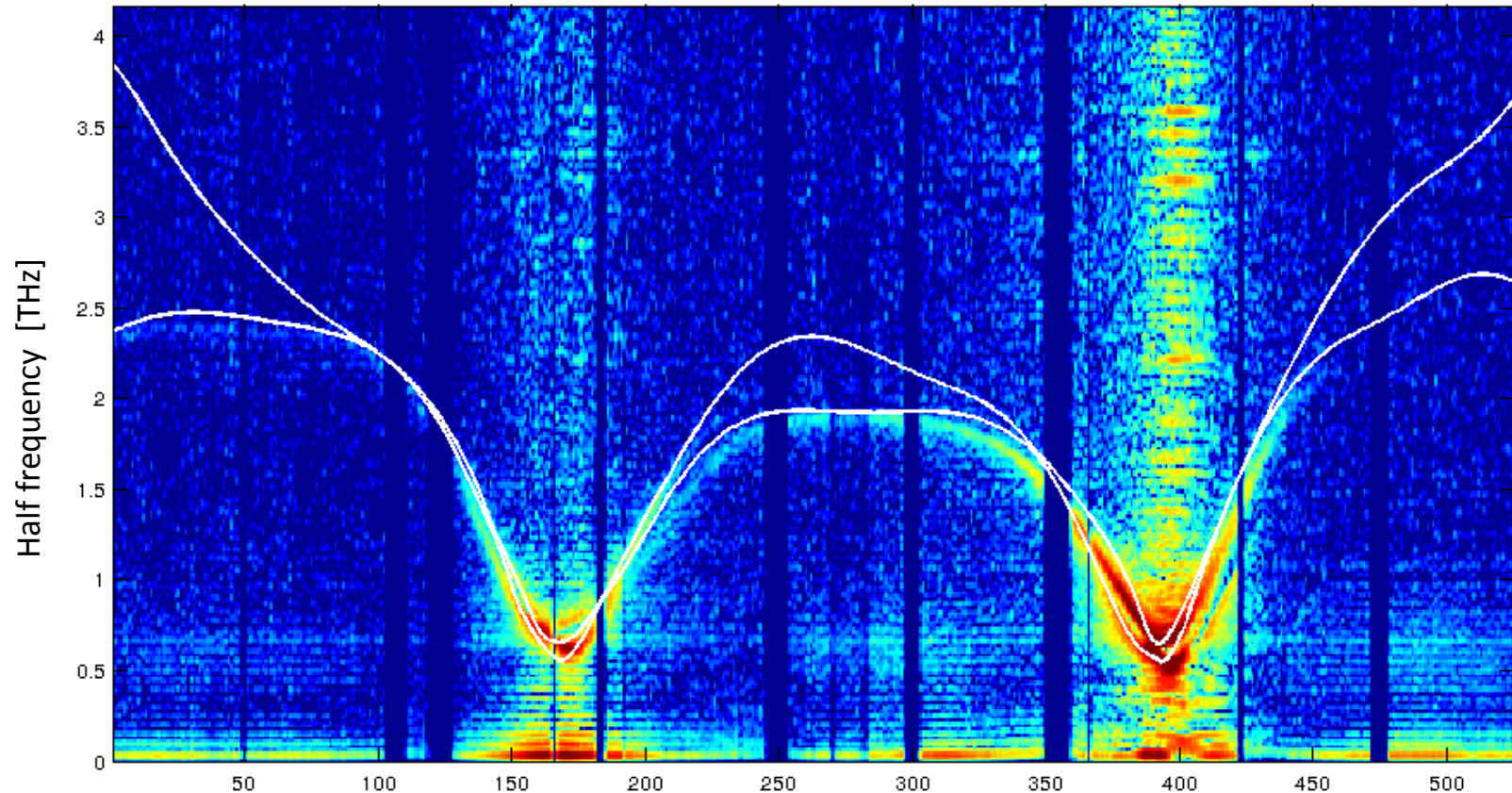
$$S(\vec{Q}; \tau) \propto \sum_{j,j'} \langle u_{j,\vec{Q}}(\tau) u_{j',-\vec{Q}}(\tau) \rangle$$

Trigo et al. Nature Physics. 9, 790, 2013

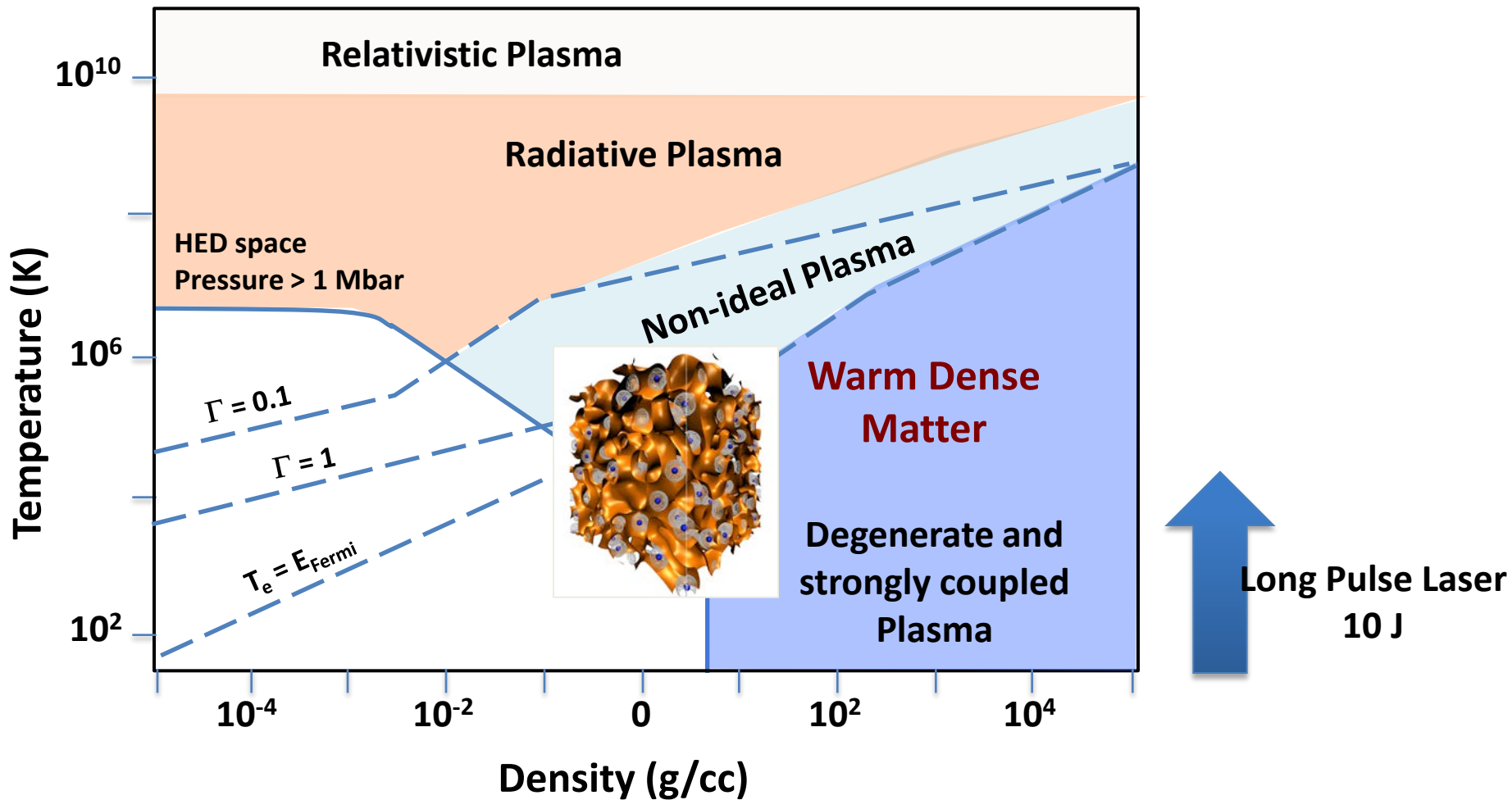
Non-equilibrium frequency (forces)



extracted TA phonon dispersion (Ge)



The High Energy Density Science space

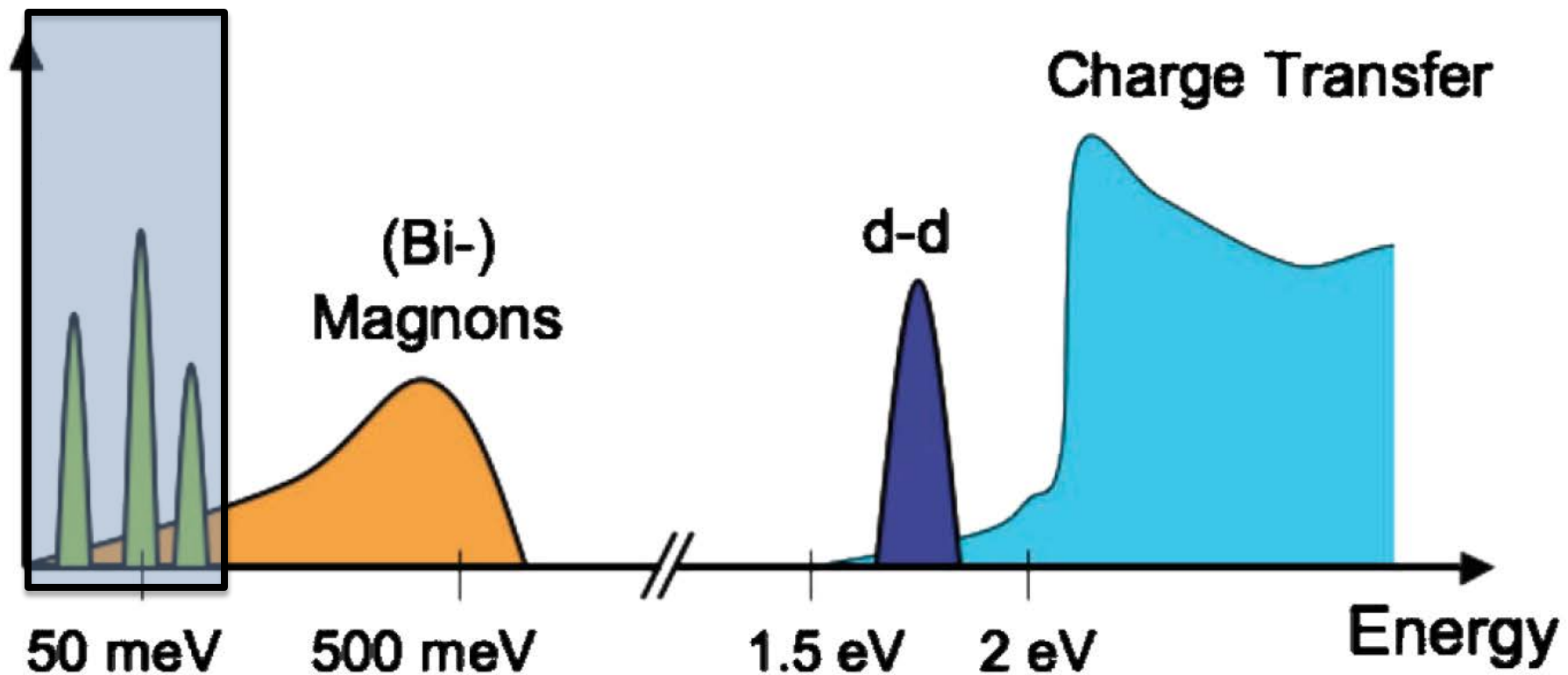


Liquids

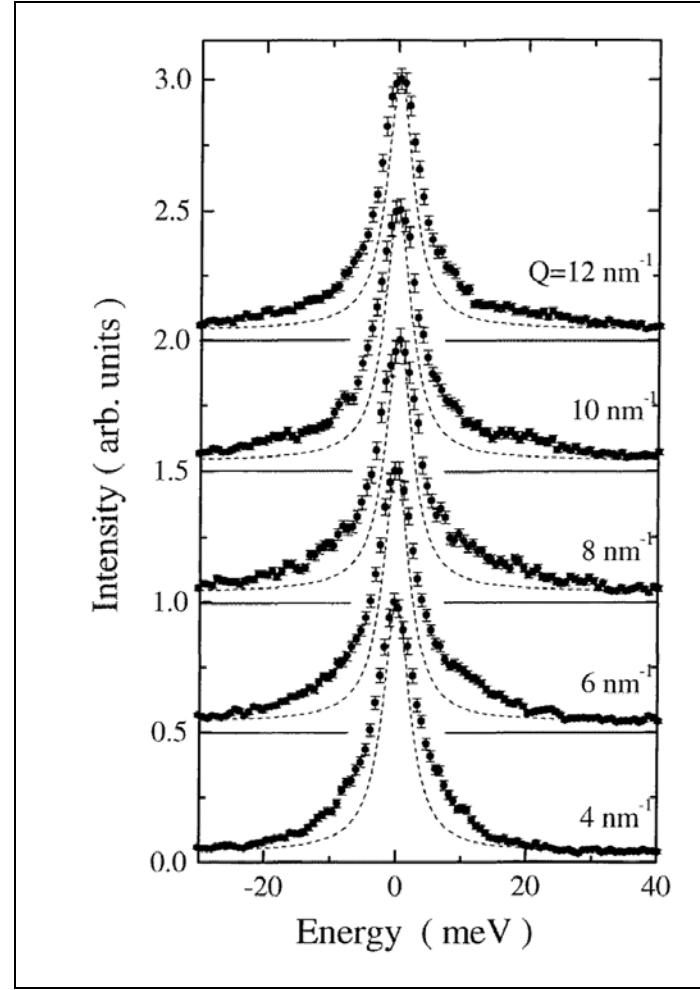


Elementary excitations

Acoustic Waves



H₂O

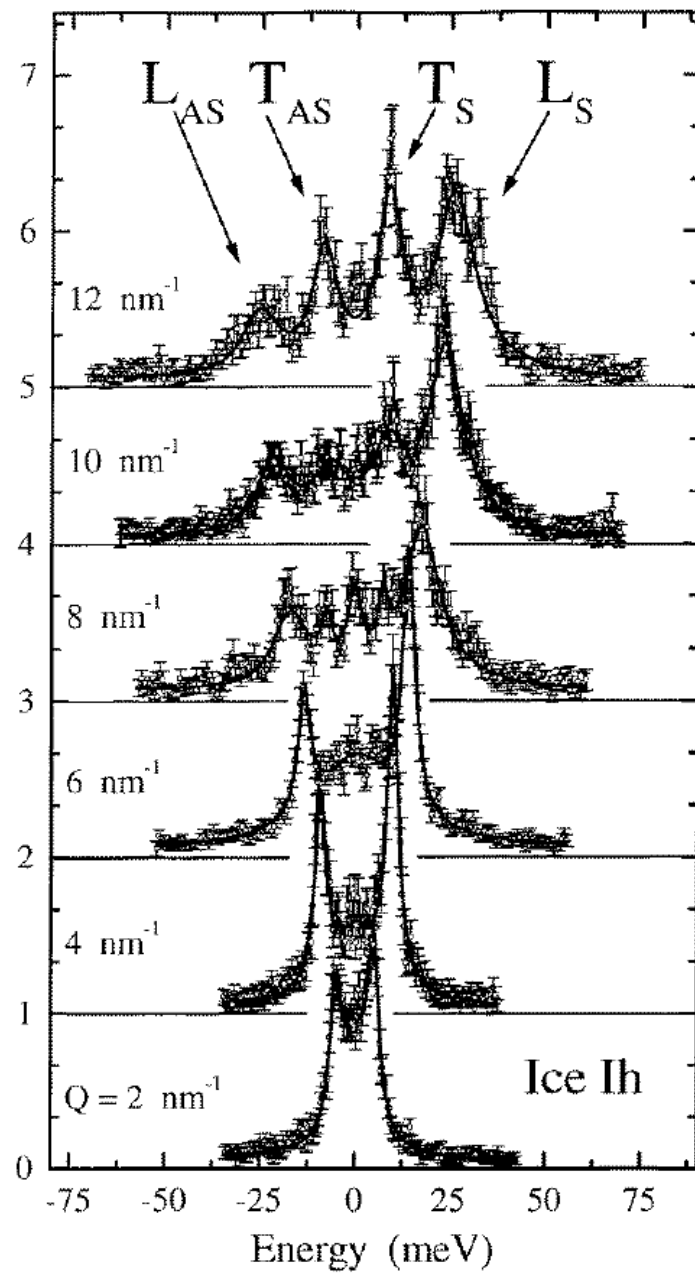


$$F(Q, E) = F_C(Q, E) + F_{DHO}(Q, E)$$

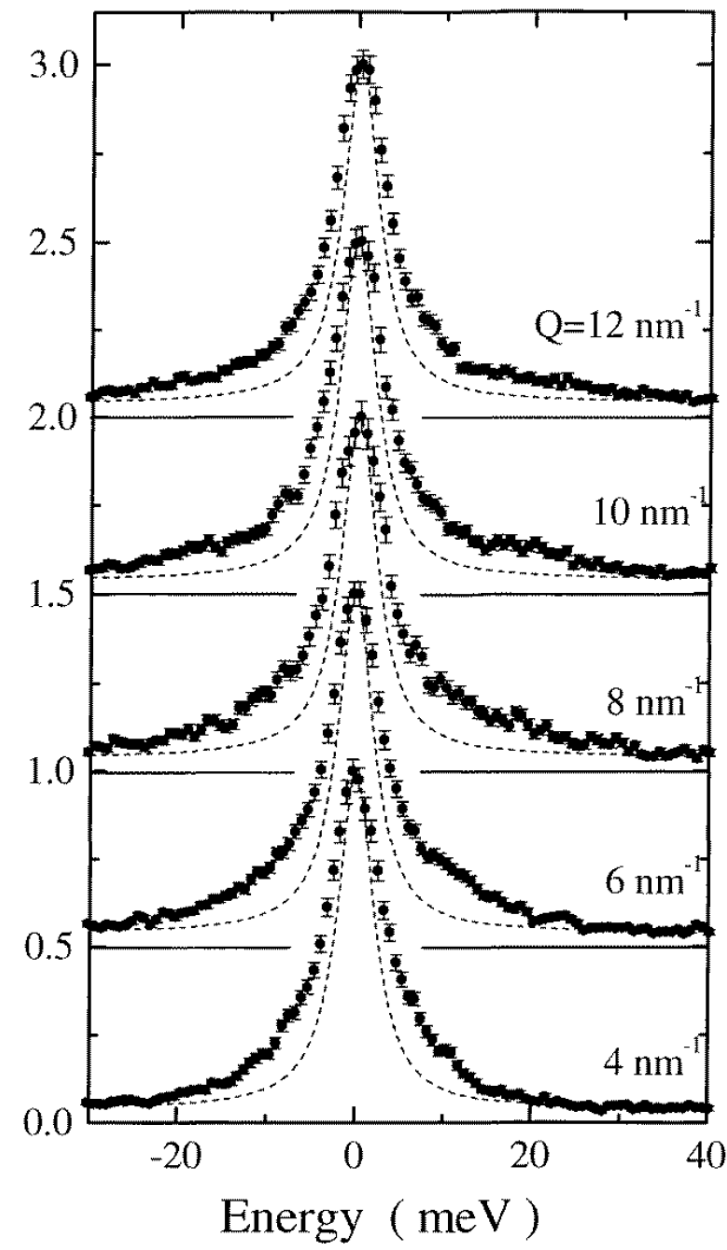
$$= \frac{1}{\pi} I_c(Q) \frac{\Gamma_c(Q)}{E^2 + \Gamma_c(Q)^2} + \frac{E[n(E) + 1]}{k_B T} \frac{1}{\pi} I(Q) \frac{\Gamma(Q)^2 \Omega(Q)}{(\Omega(Q)^2 - E^2)^2 + \Gamma(Q)^2 E^2}$$

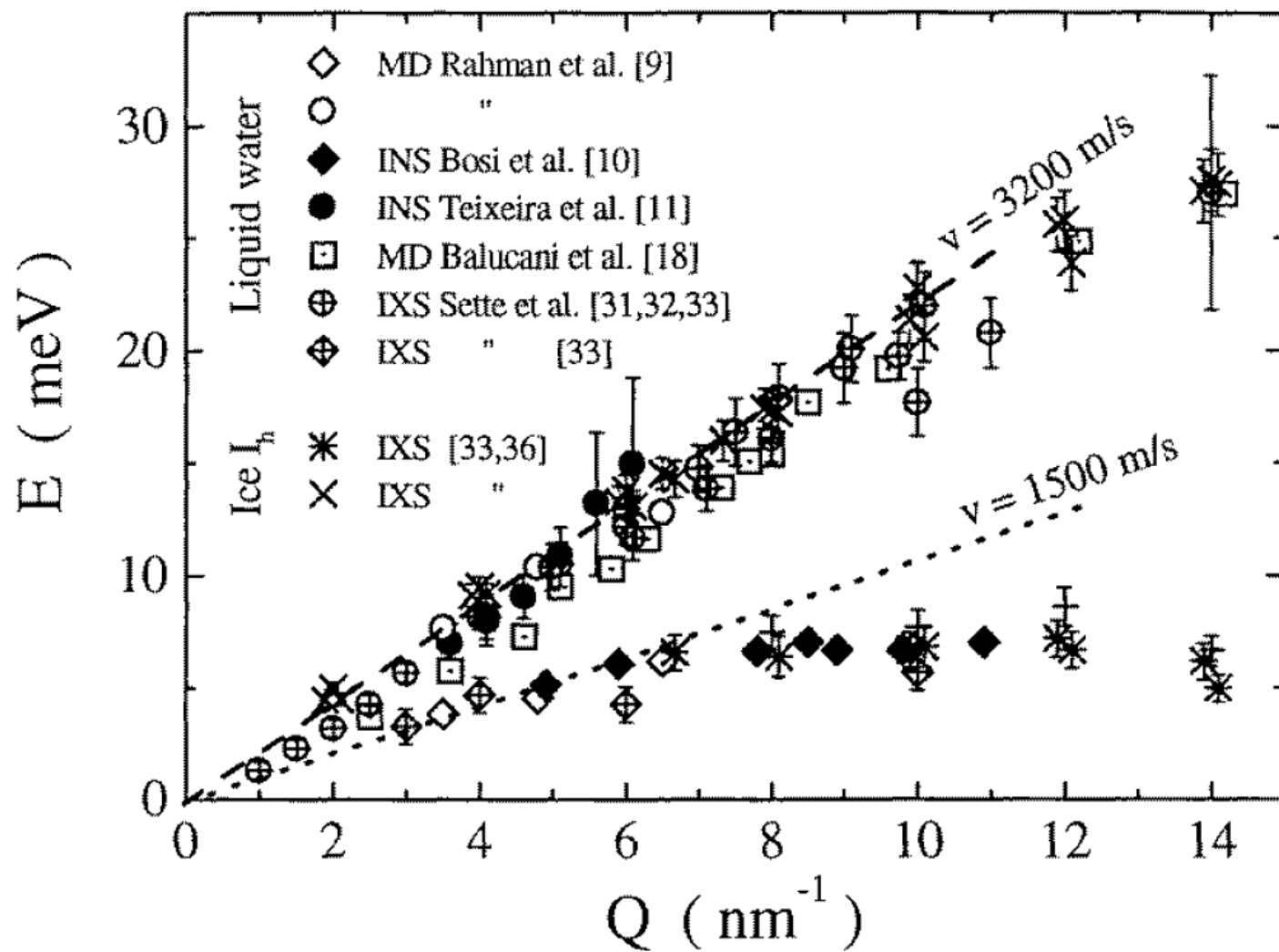


Intensity (Arbitrary Units)



Intensity (arb. units)

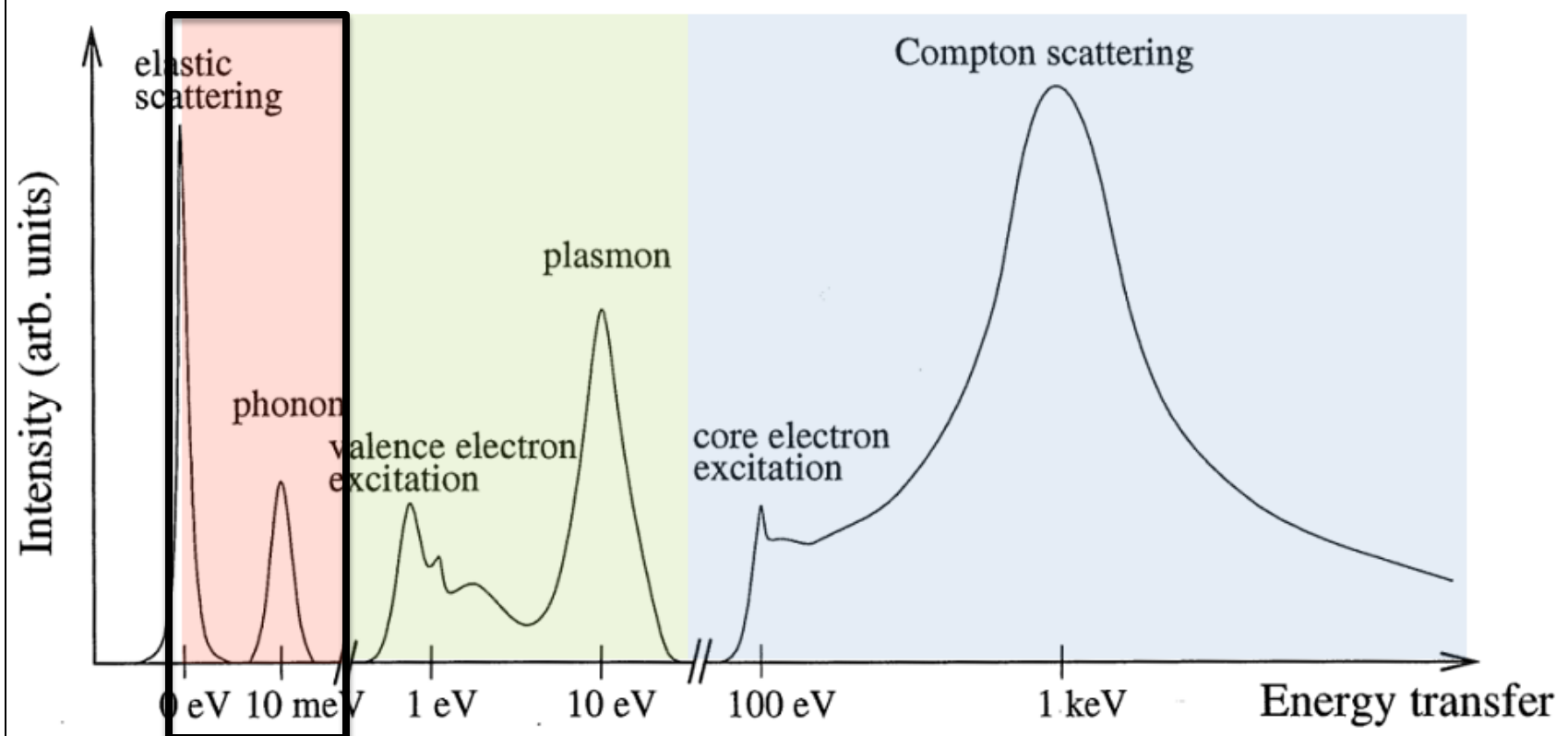




Ion-acoustic waves

Collective electron oscillations (plasmons)

Single particle regimes (Impulse Approximation)



Ion Acoustics Waves

Oxford University

T. White

N. Hartley

G. Gregori

XFEL

K. Appel

T. Tschentscher

SLAC

A. Schropp

S. Glenzer

J. Hastings

LNL

T. Doeppner

UC Berkeley

L. Fletcher

Warwick University

D. Chapman

D.O. Gericke

MEC Team

E. Galtier

E. Granados

P. Heimann

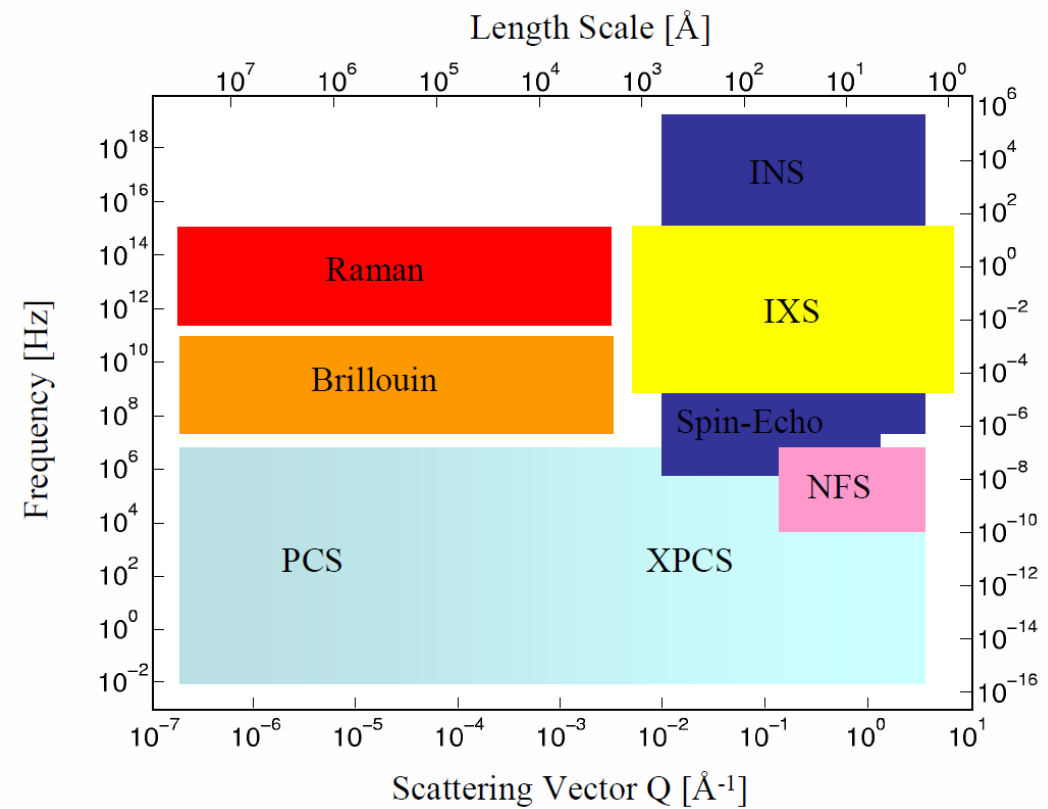
H.J. Lee

B. Nagler

U. Zastrau

University of Trento

G. Monaco

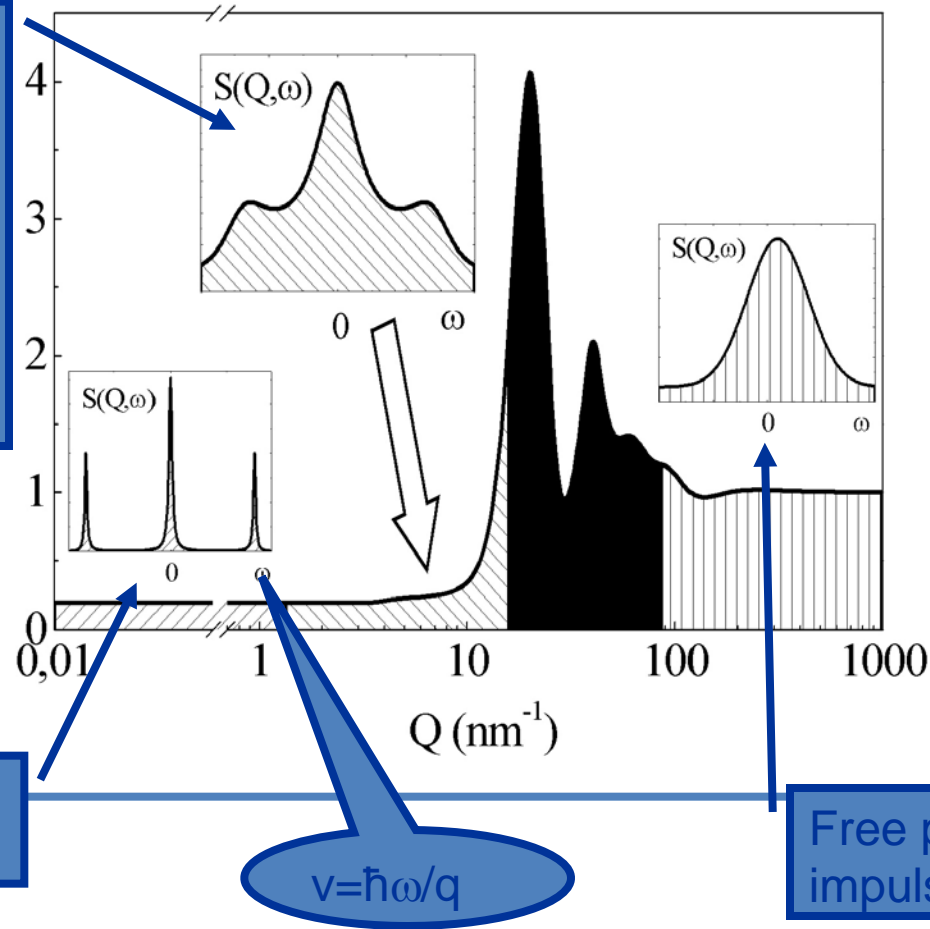


Cross-section & dynamic structure factor:

$$S(q, \omega) = S(q) \int_{-\infty}^{\infty} dt e^{-i\omega t} \Phi_q(t)$$

$$\Phi_q(t) = \frac{\langle \delta\rho_q^*(0) \delta\rho_q(t) \rangle}{\langle \delta\rho_q^*(0) \delta\rho_q(0) \rangle}$$

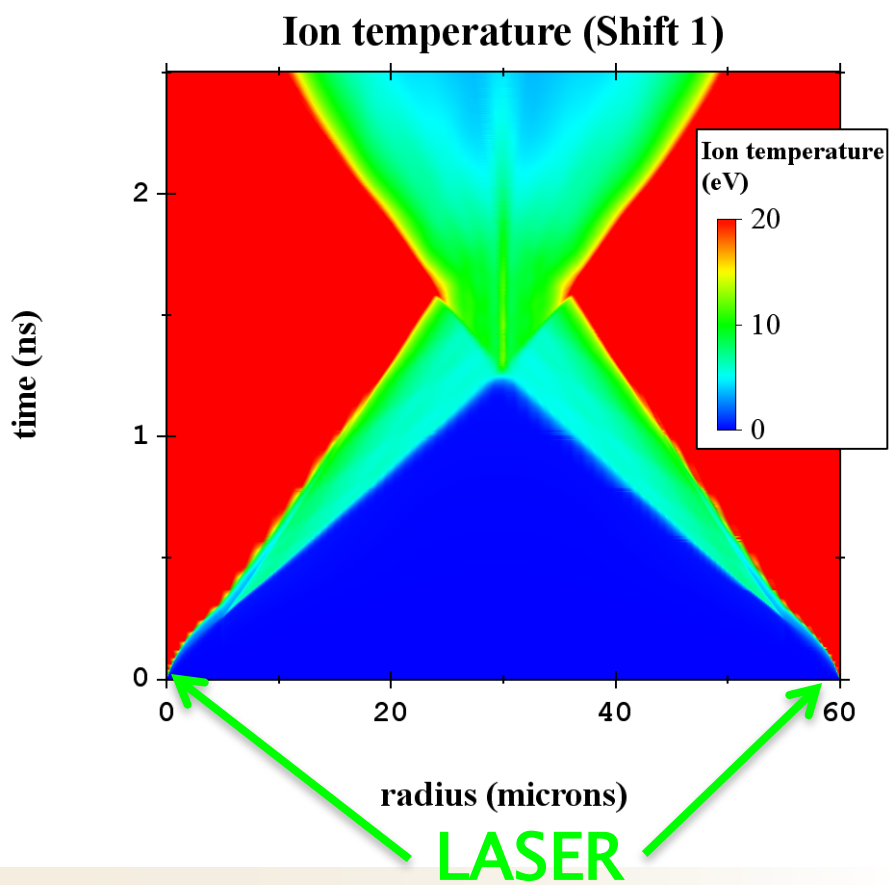
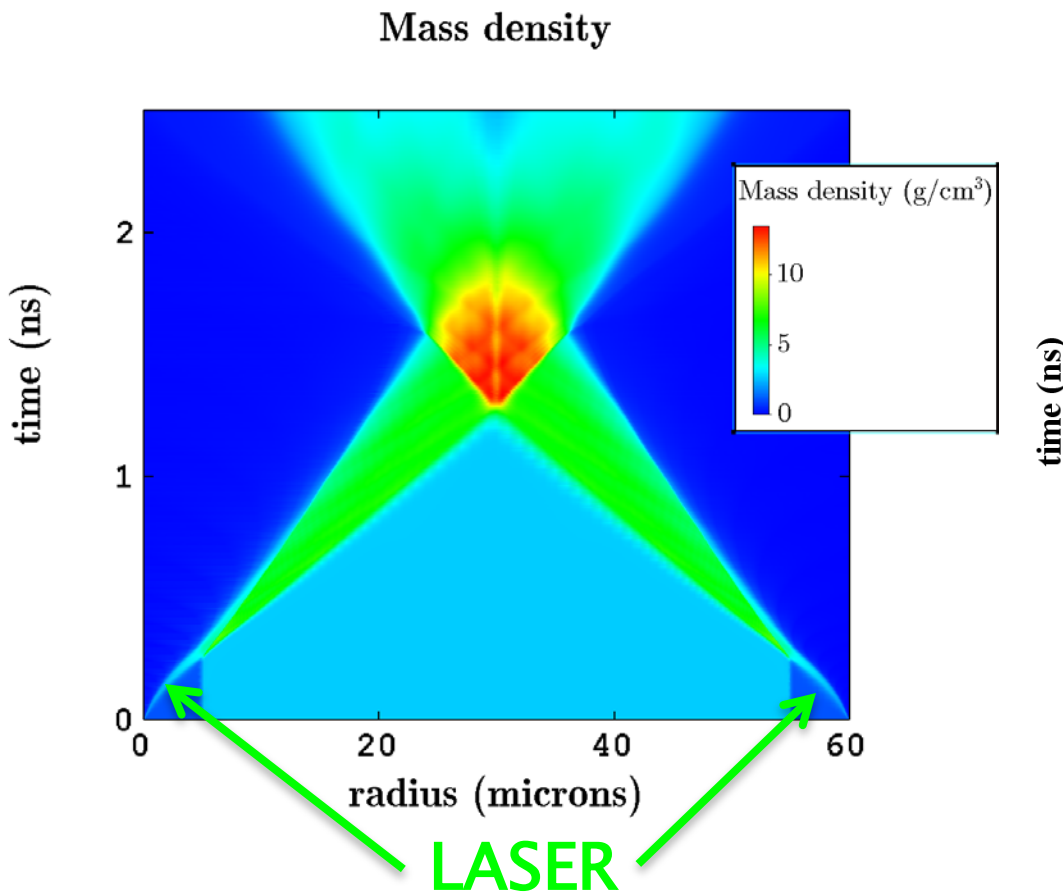
Microscopic regime
→ relaxation
processes invoked to
account for the
spectral shape and
the broadening of the
excitations

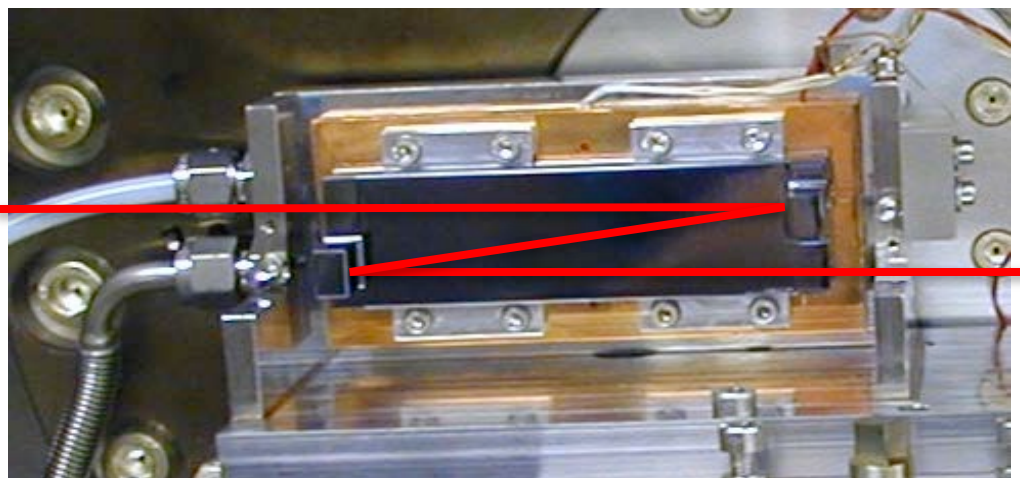
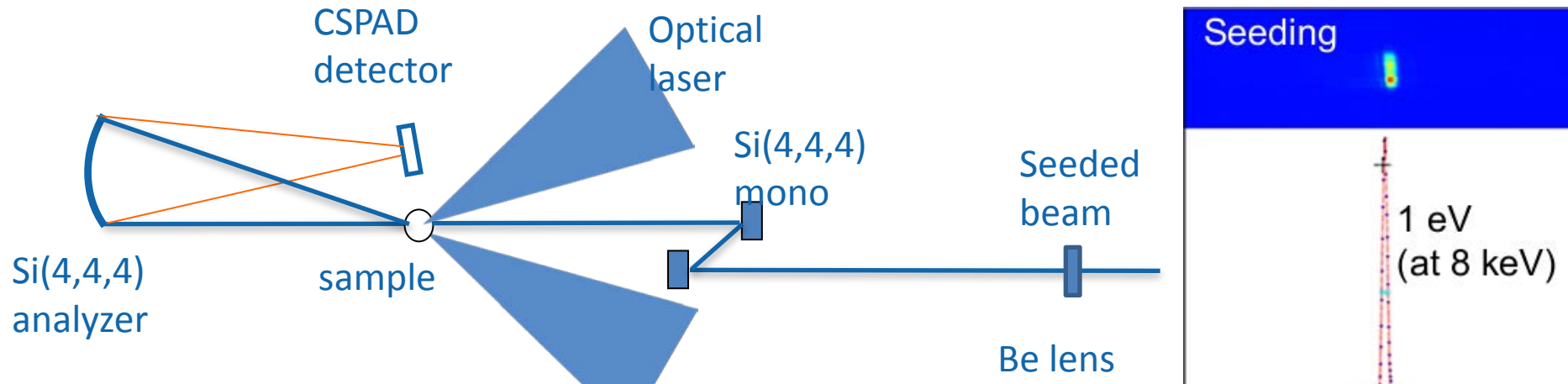


Macroscopic regime
→ hydrodynamics

Free particle regime:
impulse approximation

Double sided heating of a 50 μm Al sample (532 nm, 50 μm spot diameter & 3 ns flat top, 5 J/arm) $\Rightarrow \rho \sim 6 \text{ g/cm}^3$ & $T \sim 6 \text{ eV}$ @ 2 ns delay

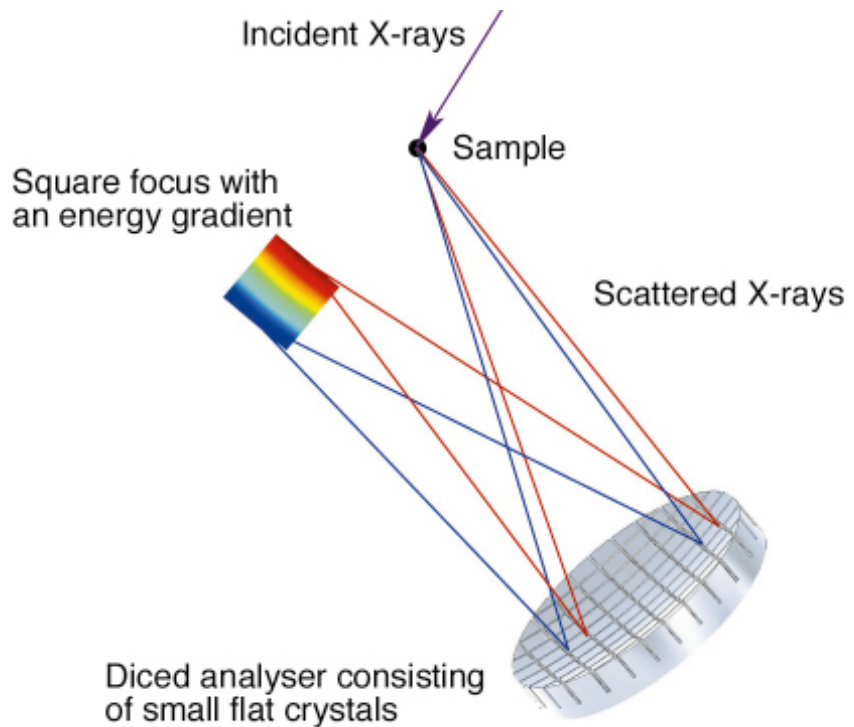




Si(4,4,4): $\Delta E/E = 5 \cdot 10^{-6}$

Working conditions:
 Bragg angle @ 9PM = 87°
 $E_{PM} = 7919.1$ eV
 $\Delta E_{PM} \sim 100$ meV

Sensitive to the seed crystal angle at the level of 0.001°



- ~10.000 cubes of $0.7 \times 0.7 \times 2.3 \text{ mm}^3$
- perfect crystal properties
- collection of sufficient solid angle

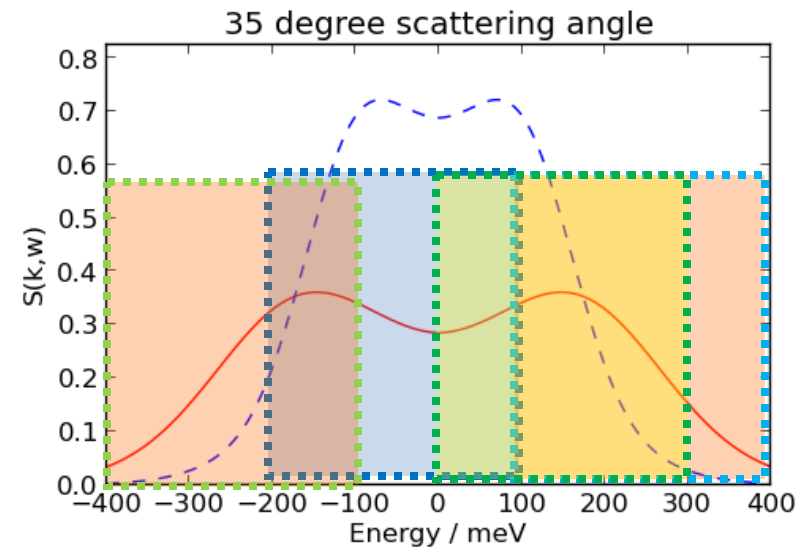
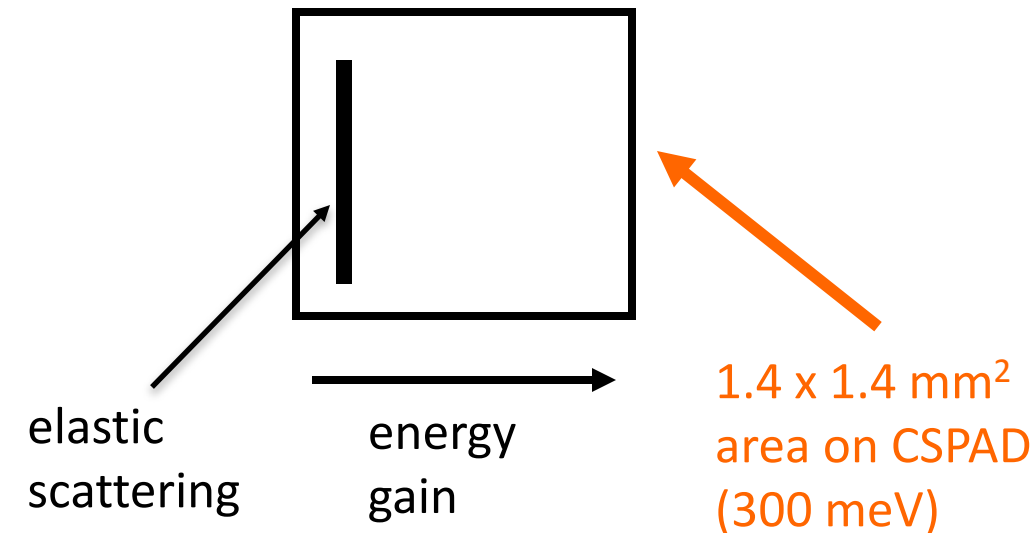
@ MEC: CSPAD ($110 \mu\text{m}$ pixel size) & diced Si(444) crystal with $R=1 \text{ m}$ & $\theta=87^\circ \Rightarrow \sim 100 \text{ meV} @ 7919 \text{ eV}$

Huotari et al., J. Synchrotron Rad. 12, 425 (2006)

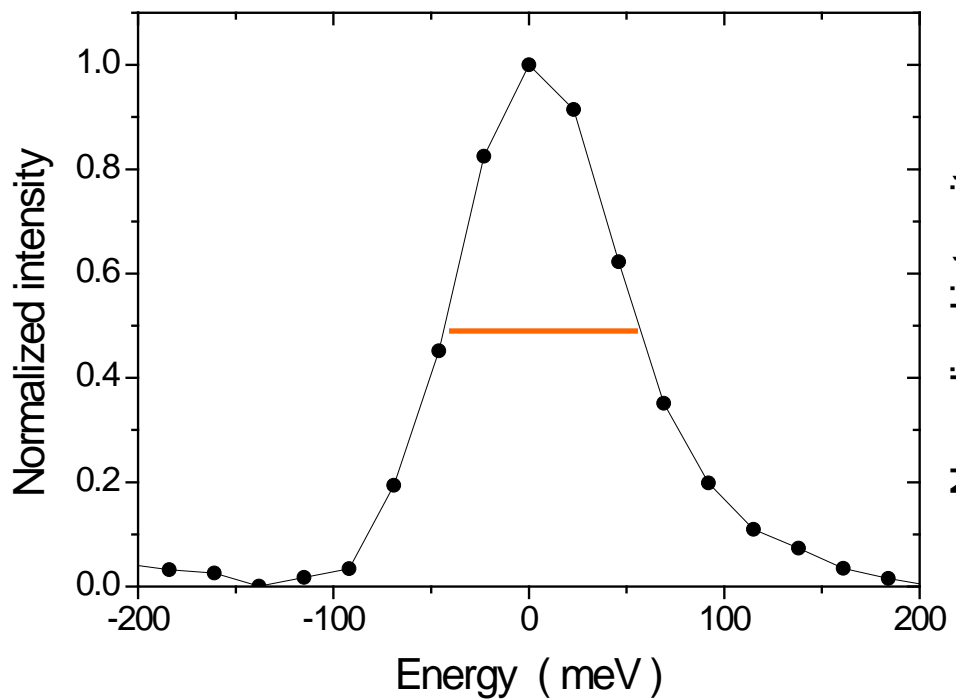
Count rate:

$$N_d \sim N_{ph} Z_A^2 S_{li}(k) n_i \sigma_T L \frac{\theta_{xtal} R_{xtal} \eta_{dect}}{4\pi}$$

- For a spectrum, ~50 photons/good shot
- For each pixel (23 meV) < 5 photons/good shot
- ~10 good shots required @ 7 min rep rate

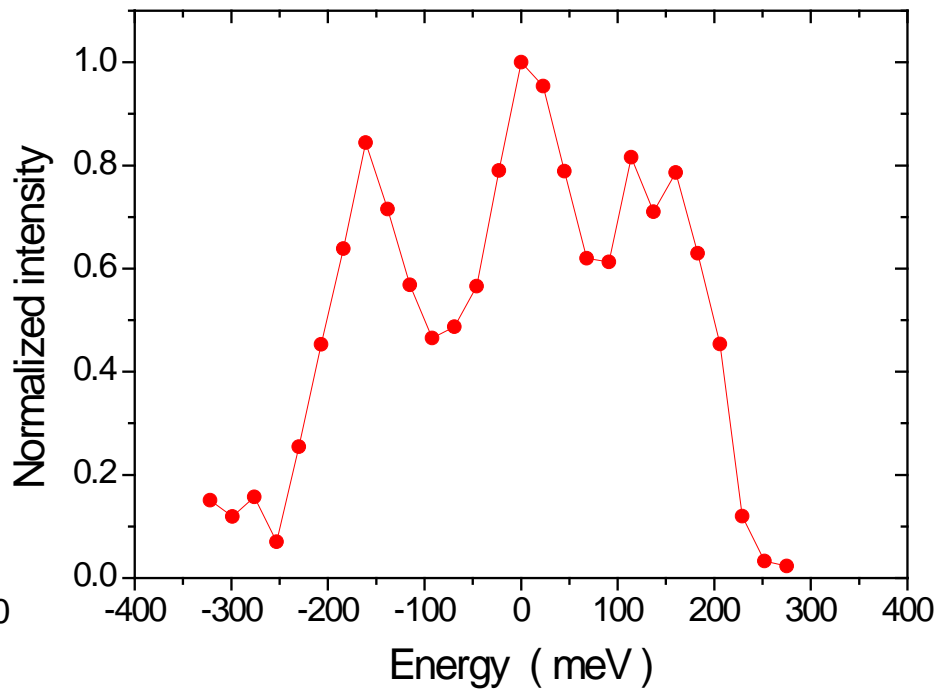


Elastic scatterer (SiO_2)



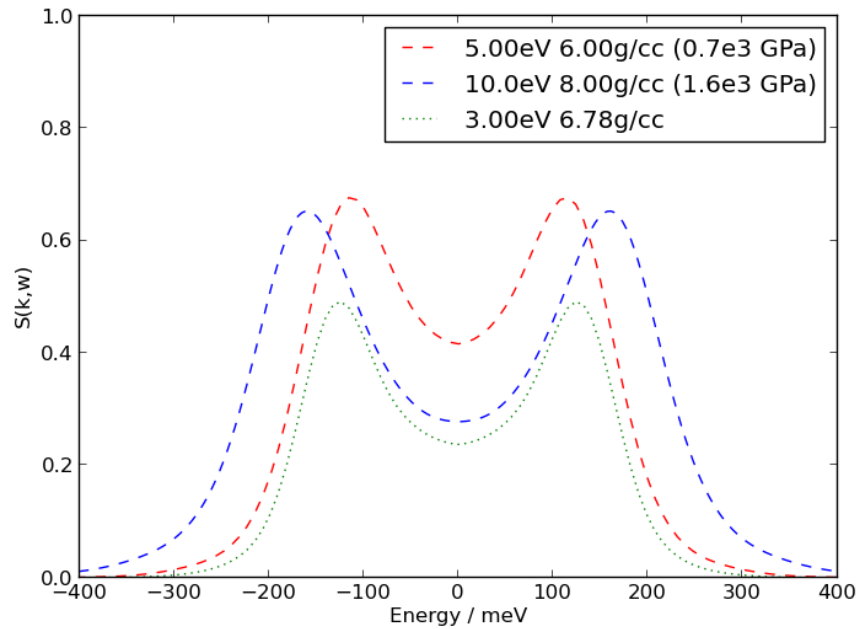
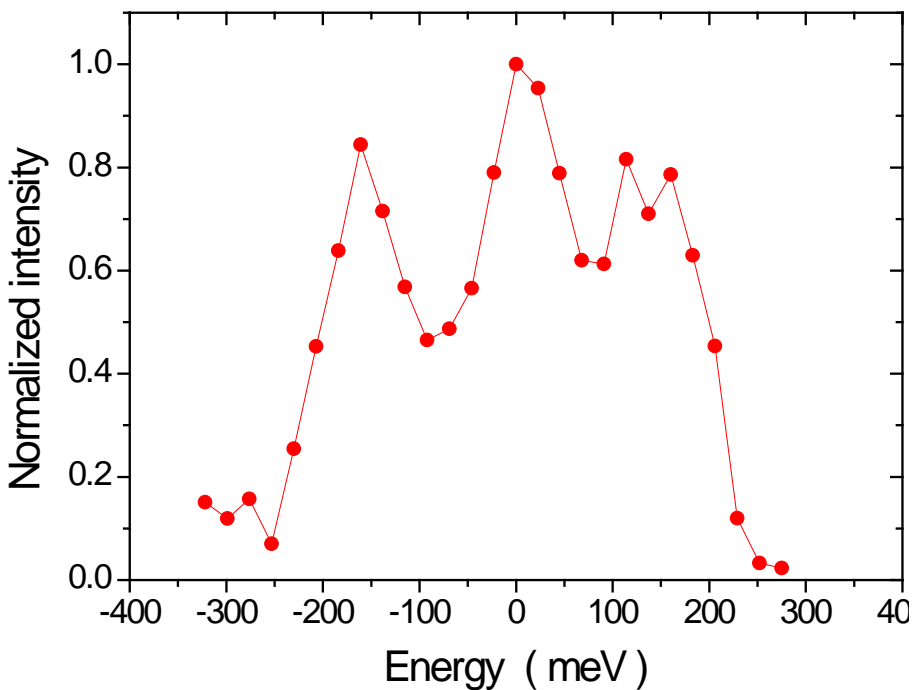
FWHM=98 meV !

$\text{Al} @ \rho = 7.0 \pm 0.9 \text{ g/cm}^3$
 $\Omega = 152 \pm 13 \text{ meV}$



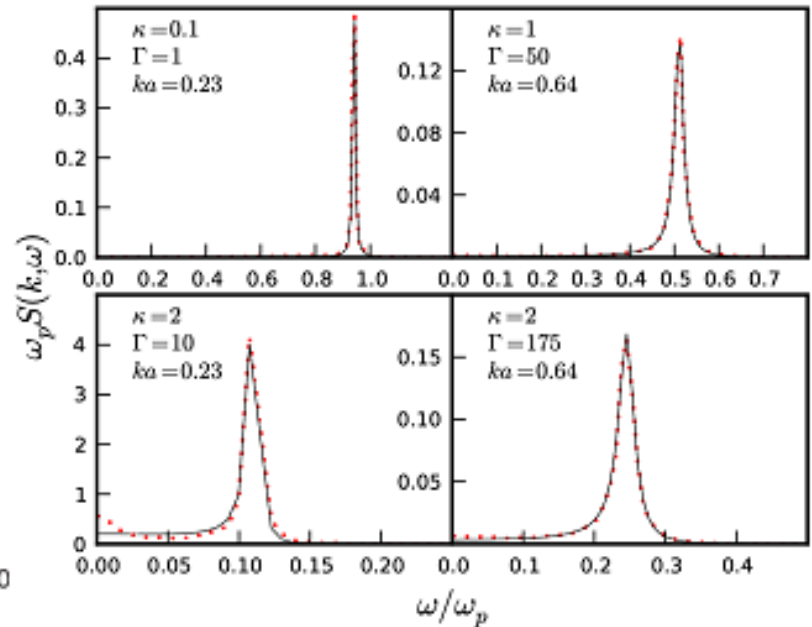
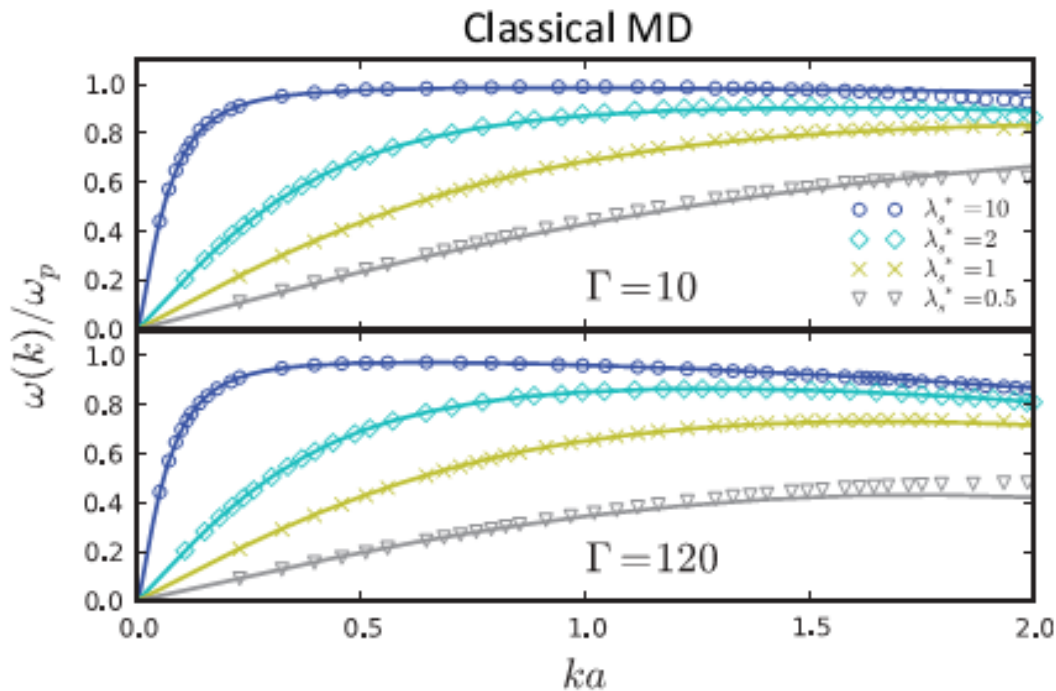
$2\theta = 30^\circ, Q = 2.1 \text{ \AA}^{-1}$
 $Q_0 = 3.7 \pm 0.1 \text{ \AA}^{-1}; Q/Q_0 = 0.57$

Comparing experimental results and simulations:



ab-initio quantum MD simulations (OF-DFT) describe pretty well the inelastic components. Where is the elastic one?

- Experiments & simulations show there is a finite range of wave-numbers where the hydrodynamics approximation holds.
- At larger wave-numbers, hydrodynamics models still reproduce experiments & simulations if k-dependent transport properties are used.

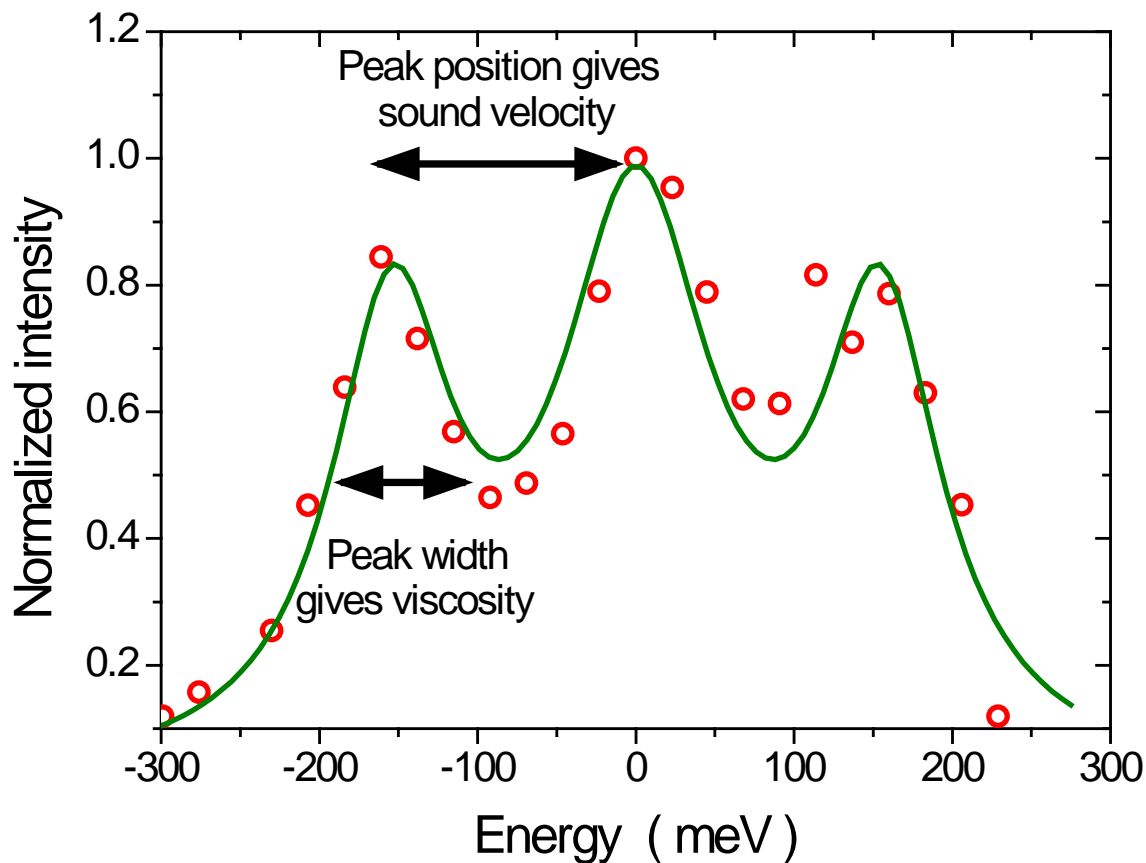


Mithen et al., PRE 83, 015401(R) (11)

Rayleigh peak

$$\frac{S(k,\omega)}{S(k)/2\pi} = \frac{\gamma}{\gamma-1} \frac{c_s^2 k^2}{\omega_m^2} \frac{2D_T k^2}{\omega^2 + (D_T k^2)^2} + \frac{\omega_{m\gamma}}{\omega_m} \left[\frac{\sigma k^2}{(\omega + \omega_m)^2 + (\sigma k^2)^2} + \frac{\sigma k^2}{(\omega - \omega_m)^2 + (\sigma k^2)^2} \right]$$

Brillouin peaks



Fit results

viscosity:

$\sigma \sim 5 \text{ mPa s}$

sound velocity:

$v \sim 11 \text{ km s}^{-1}$

Liquids (Water)

$$F(Q, E) = F_C(Q, E) + F_{DHO}(Q, E)$$

$$= \frac{1}{\pi} I_c(Q) \frac{\Gamma_c(Q)}{E^2 + \Gamma_c(Q)^2} + \frac{E[n(E) + 1]}{k_B T} \frac{1}{\pi} I(Q) \frac{\Gamma(Q)^2 \Omega(Q)}{(\Omega(Q)^2 - E^2)^2 + \Gamma(Q)^2 E^2}.$$



$$\frac{S(k, \omega)}{S(k)/2\pi} = \frac{\gamma}{\gamma - 1} \frac{c_s^2 k^2}{\omega_m^2} \frac{2D_T k^2}{\omega^2 + (D_T k^2)^2} + \frac{\omega_{m\gamma}}{\omega_m} \left[\frac{\sigma k^2}{(\omega + \omega_m)^2 + (\sigma k^2)^2} + \frac{\sigma k^2}{(\omega - \omega_m)^2 + (\sigma k^2)^2} \right]$$

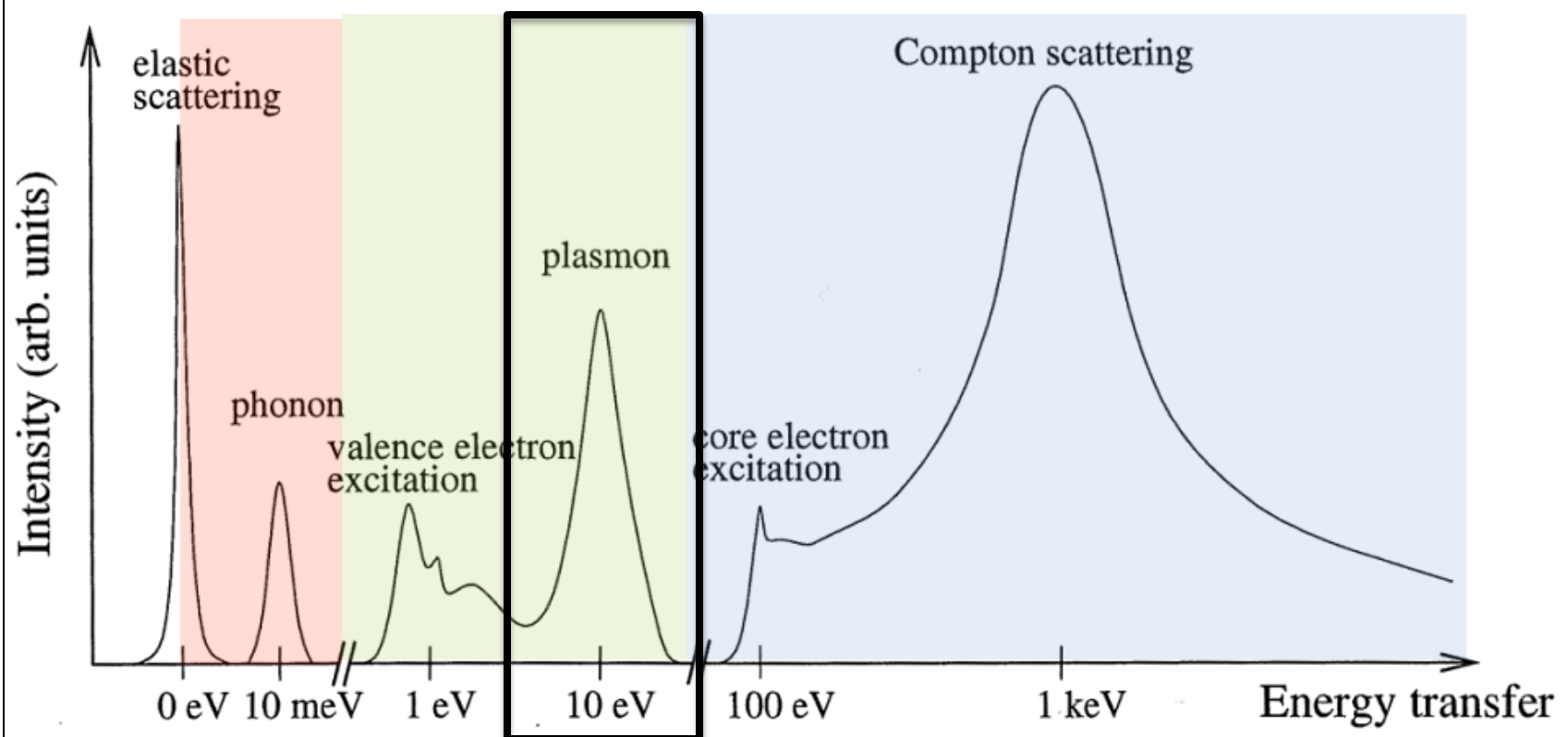
Ion Acoustic Waves (WD Aluminum)

Plasmons

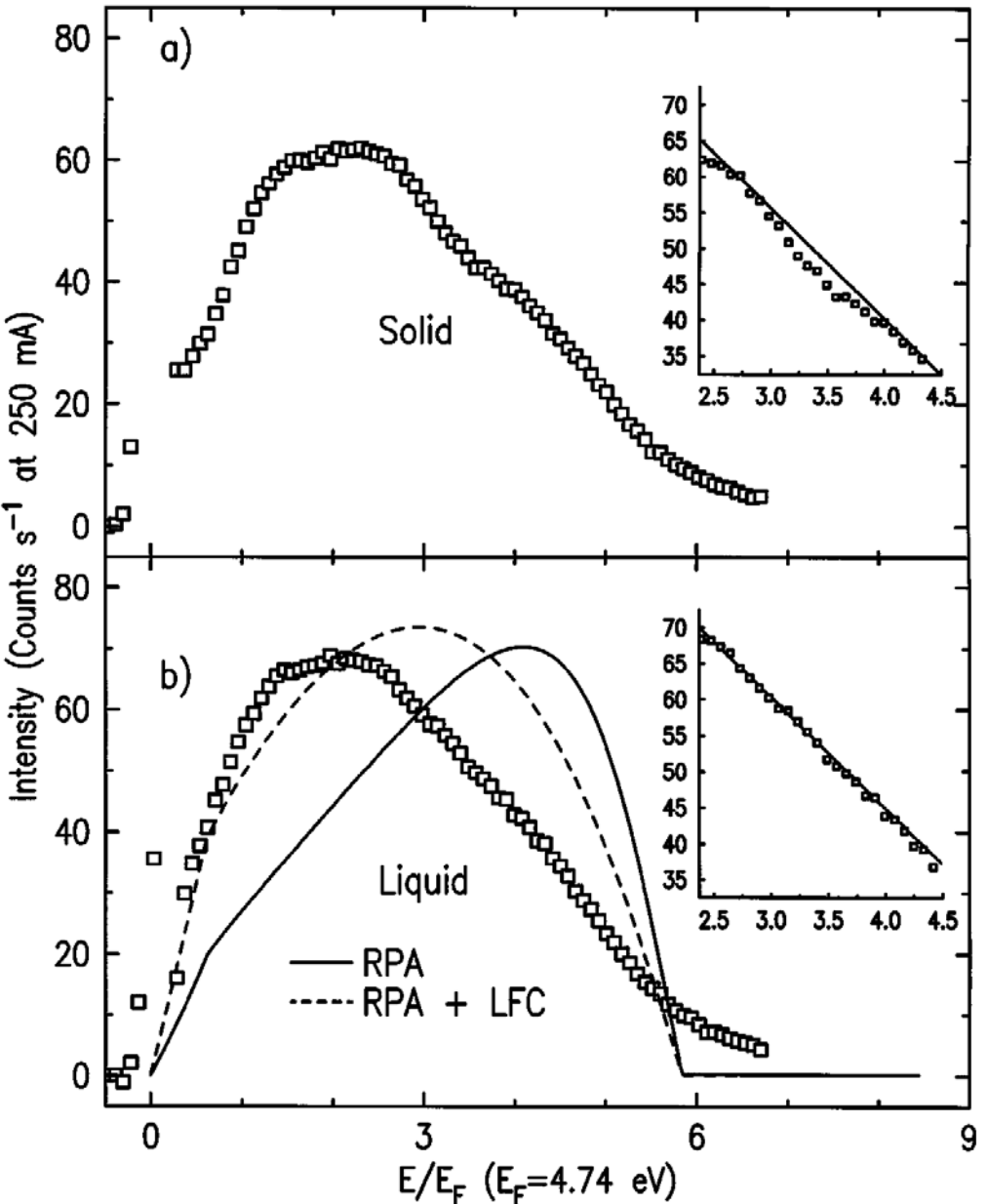
Ion-acoustic waves

Collective electron oscillations (plasmons)

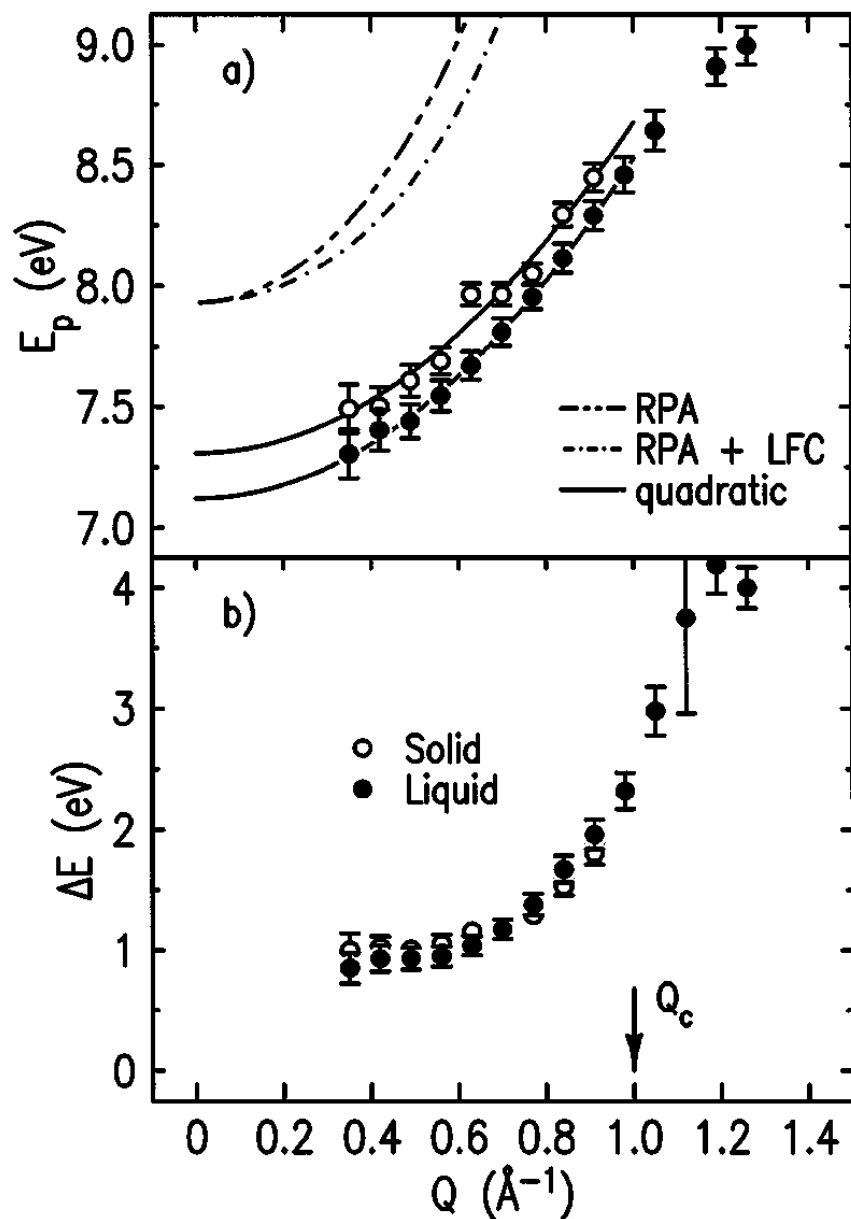
Single particle regimes (Impulse Approximation)



Lithium $Q=1.81 \text{ \AA}^{-1}$, $Q/Q_F=1.61$

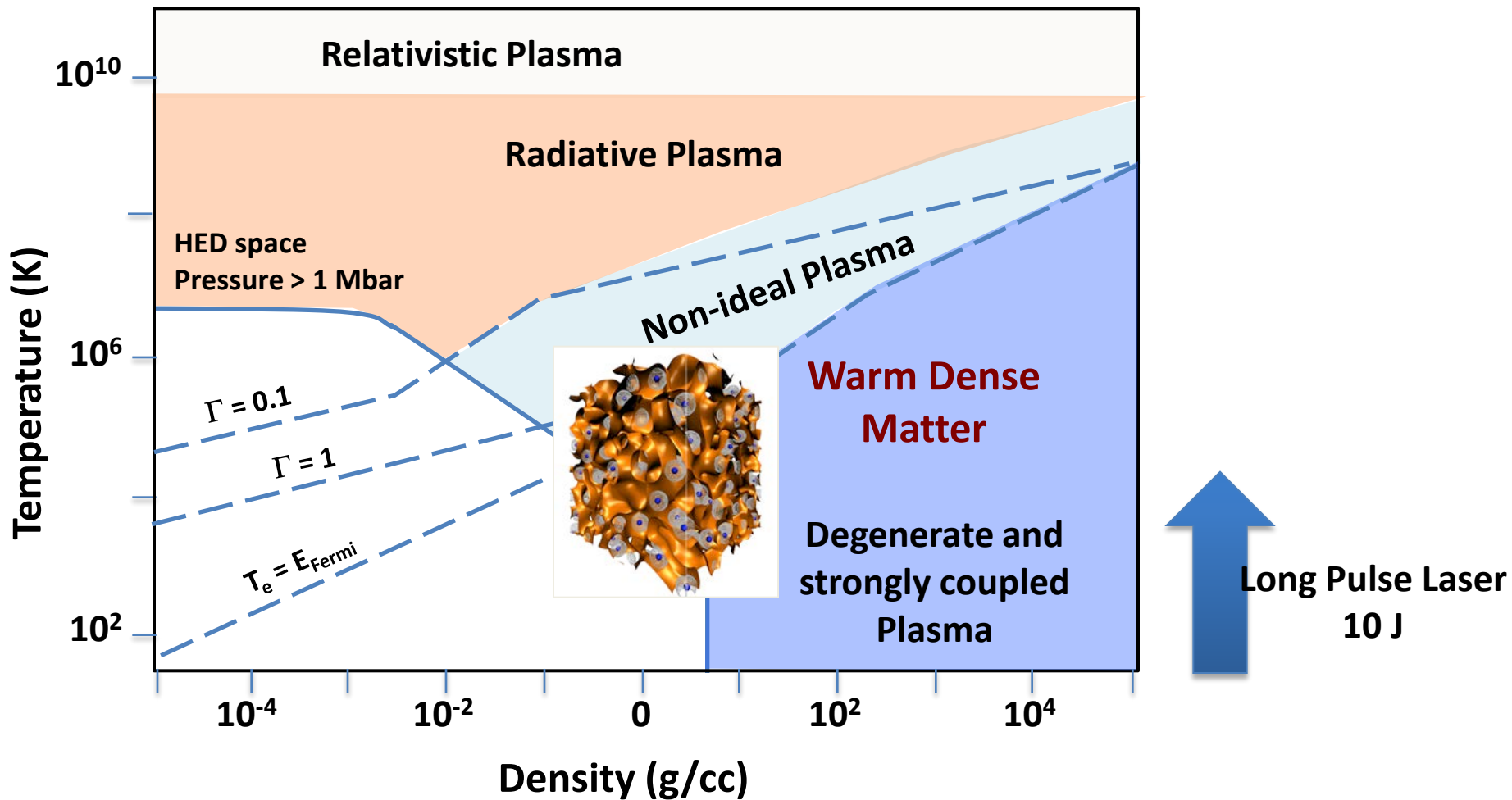


Plasmons in Lithium



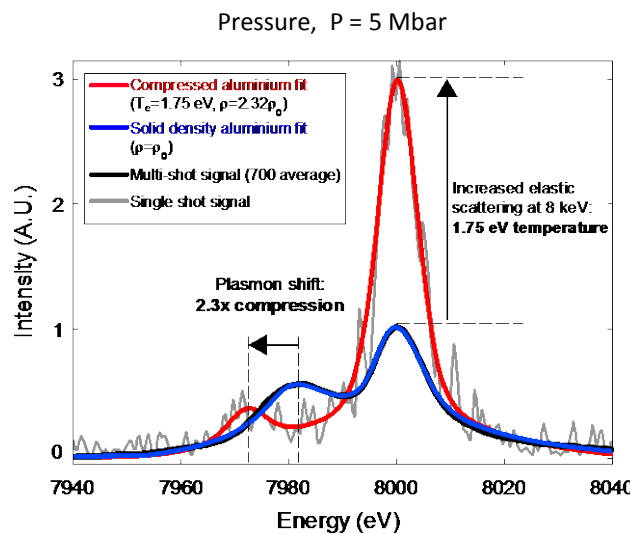
Hill, J. P., et al. "Inelastic X-ray scattering study of solid and liquid Li and Na." Physical review letters 77, 3665 (1996)

The High Energy Density Science space



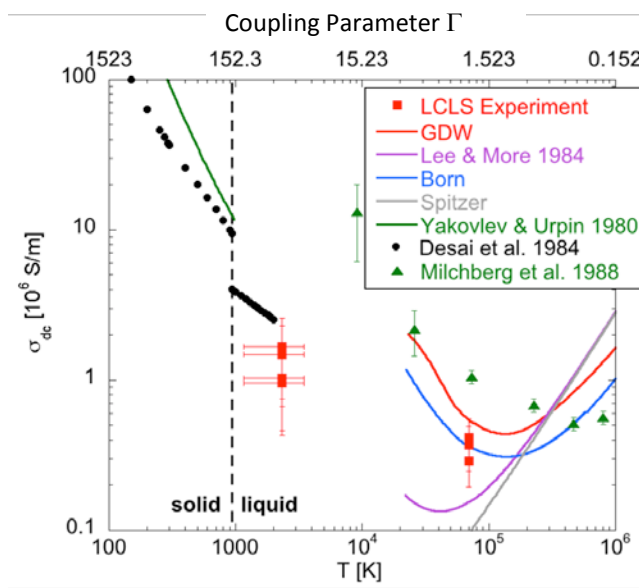
Inelastic x-ray scattering measures physical properties of warm dense matter

Single-shot plasmons determine compression



- *Density, Temperature*
- Characterize laser shock-compressed Al
 - Compressed solid,
 - Co-existence phase
 - Warm Dense Matter

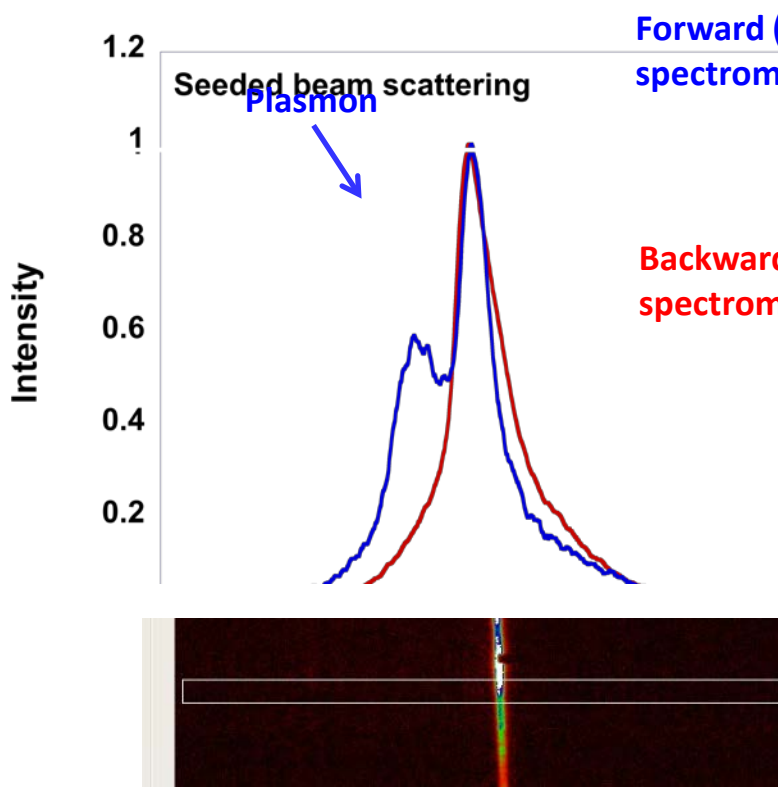
Plasmon damping determines conductivity



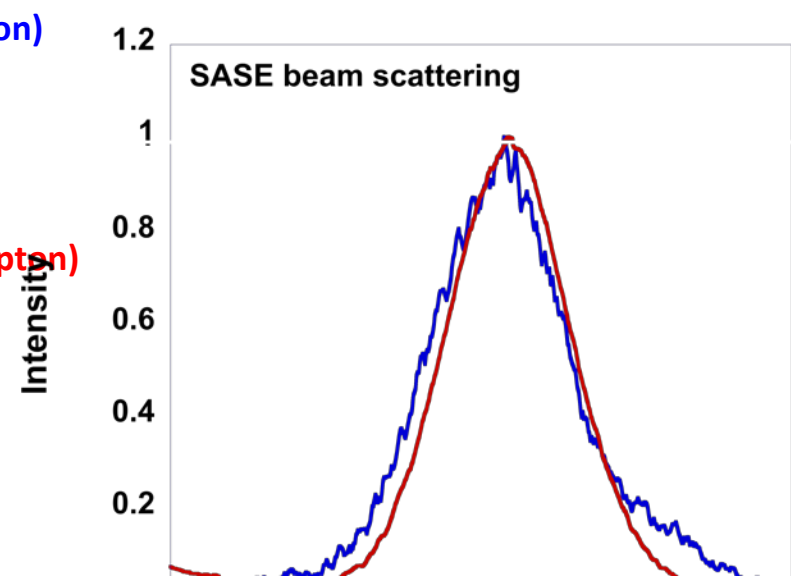
- First *Conductivity* measurements with independent T_e, n_e data
- Solid Al at $T = 6$ eV

High resolution x-ray scattering observations of plasmons in Al using the seeded beam at 8 keV

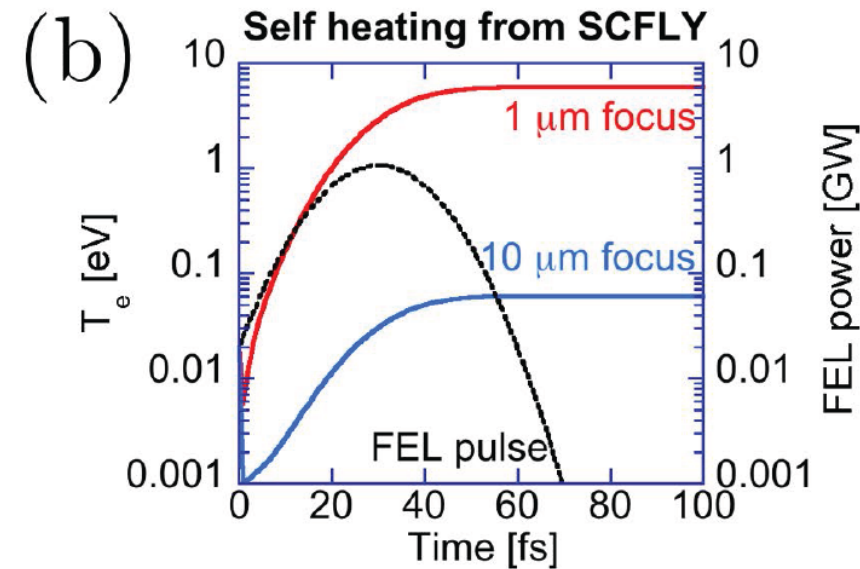
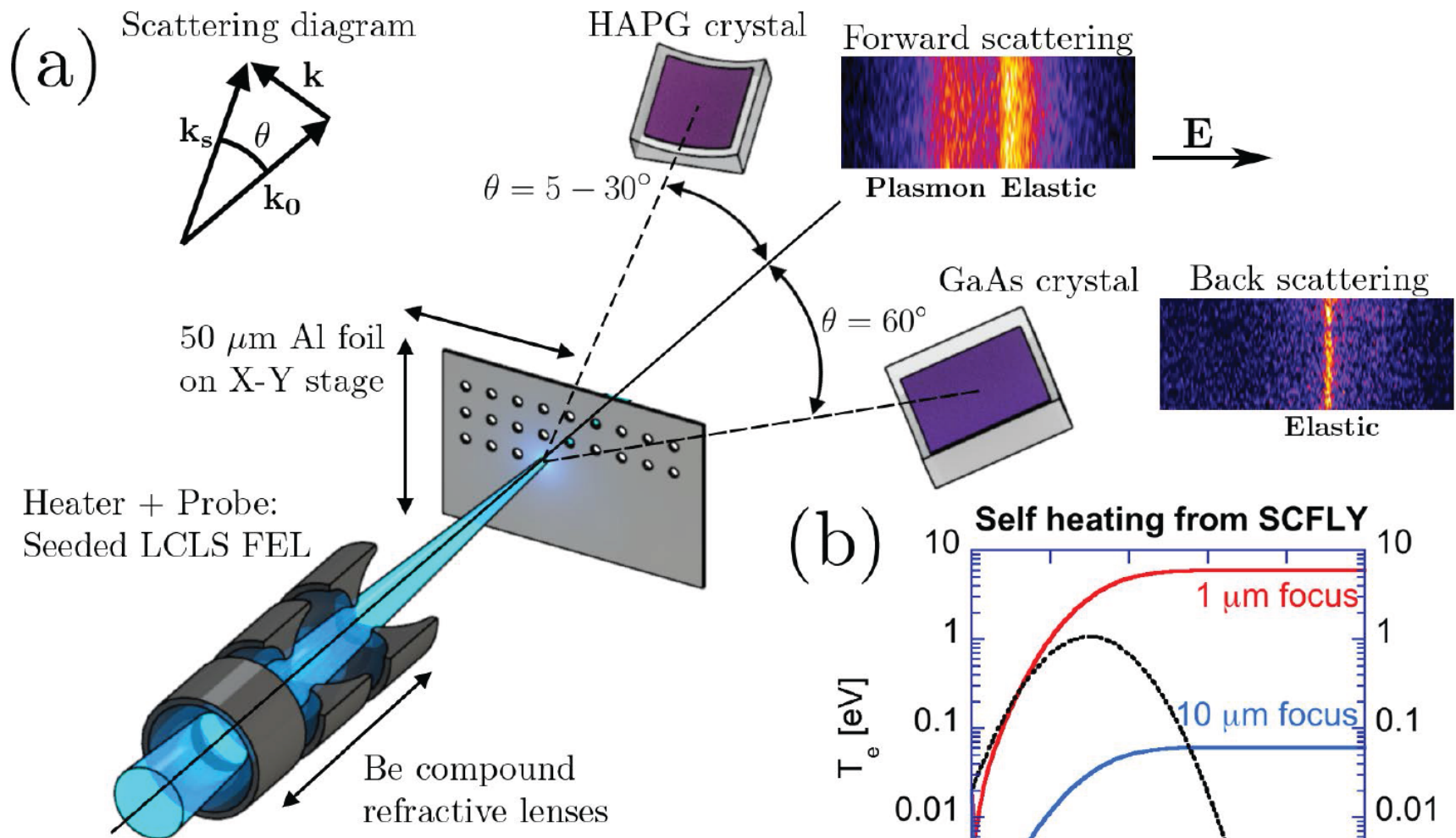
X-ray scattering from isochorically heated Al with seeded beam resolves plasmons



Seeded



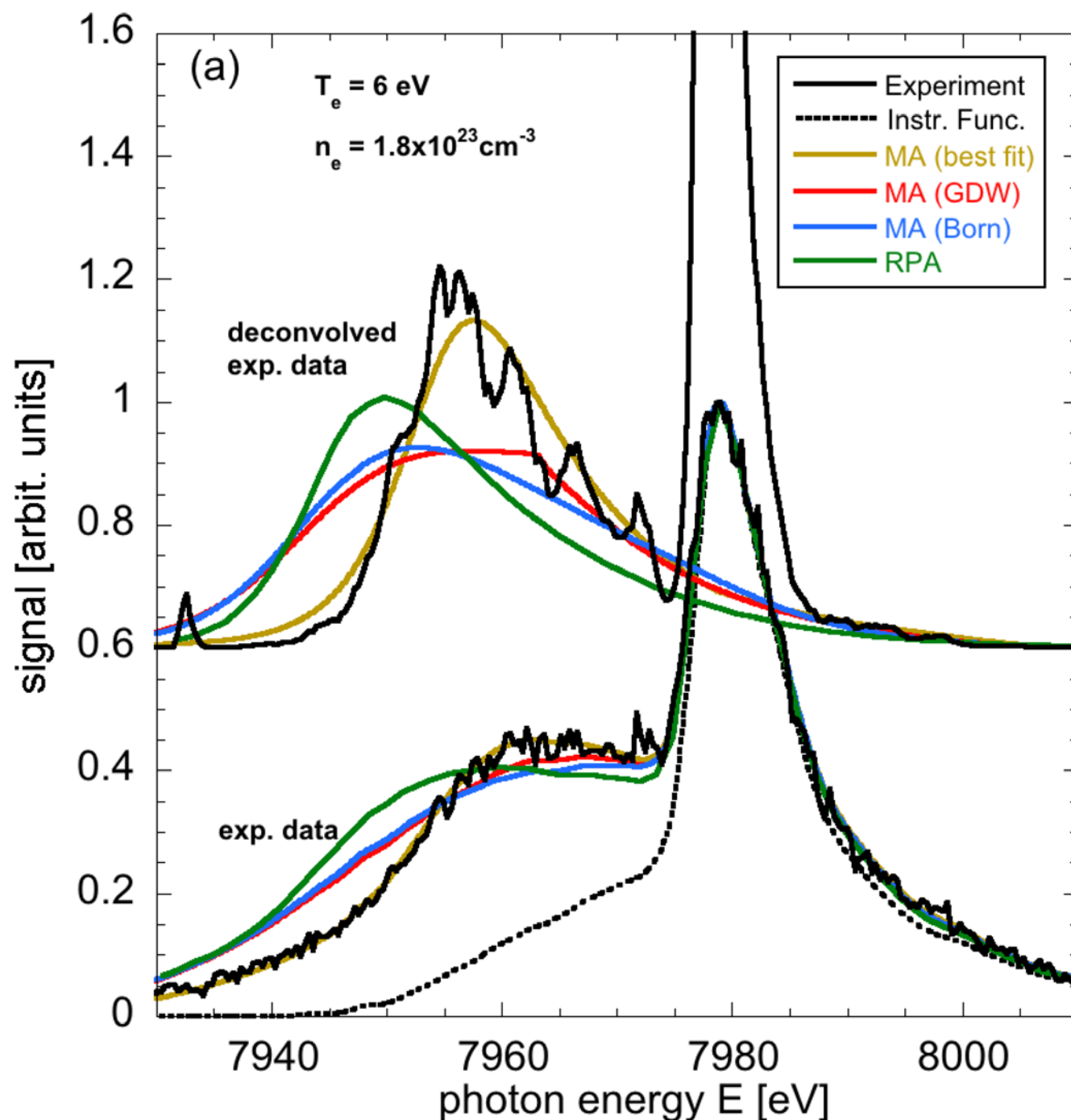
SASE

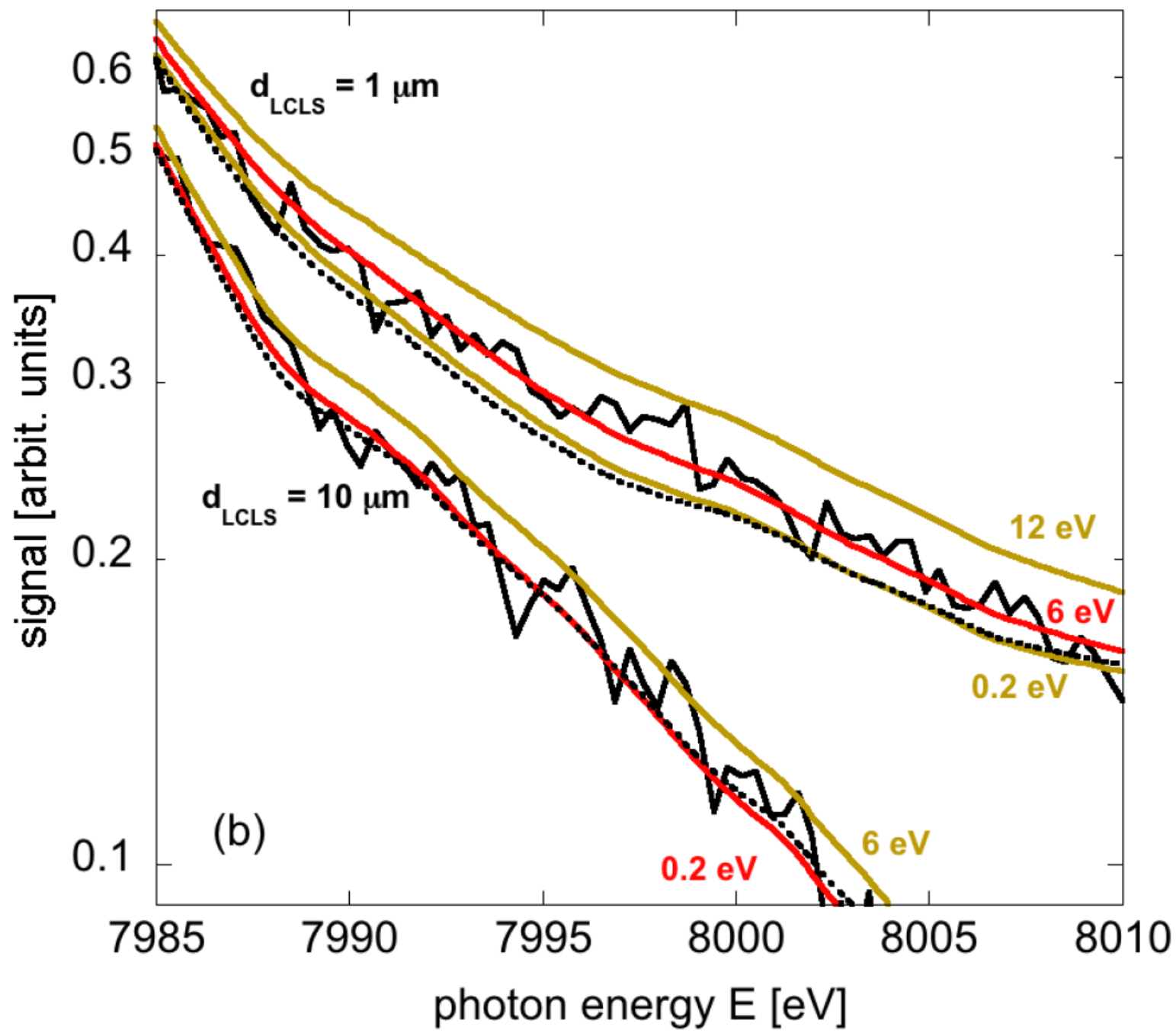


Detailed balance

$$\frac{S_{ee}^0(k, \omega)}{S_{ee}^0(-k, -\omega)} = \exp(-h\omega / k_B T_e)$$

$S_{ee}^0(k, \omega)$ Is the dynamic structure factor of the free electrons





Summary

Inelastic x-ray scattering using FELs provides unique information that is crucial to understanding important properties of condensed matter

